Sensitivity Analysis of the Interfrequency Correlation of Synthetic Ground Motions to Pseudodynamic Source Models

Seok Goo Song, Mathieu Causse, Jeff Bayless

Seismological Research Letters

Sensitivity Analysis of the Inter-frequency Correlation of Synthetic Ground Motions to Pseudo-dynamic Source Models

--Manuscript Draft--

Manuscript Number:	SRL-D-20-00181R2
Full Title:	Sensitivity Analysis of the Inter-frequency Correlation of Synthetic Ground Motions to Pseudo-dynamic Source Models
Article Type:	Article - Regular Section
Corresponding Author:	Seok Goo Song, Ph.D. Korea Institute of Geoscience and Mineral Resources Daejeon, KOREA, REPUBLIC OF
Corresponding Author Secondary Information:	
Corresponding Author's Institution:	Korea Institute of Geoscience and Mineral Resources
Corresponding Author's Secondary Institution:	
First Author:	Seok Goo Song, Ph.D.
First Author Secondary Information:	
Order of Authors:	Seok Goo Song, Ph.D.
	Mathieu Causse
	Jeff Bayless
Order of Authors Secondary Information:	
Manuscript Region of Origin:	KOREA, REPUBLIC OF
Abstract:	Given the deficiency of recorded strong ground motion data, it is important to understand the effects of earthquake rupture processes on near-source ground motion characteristics and to develop physics-based ground motion simulation methods for advanced seismic hazard assessments. Recently, the inter-frequency correlation of ground motions has become an important element of ground motion predictions. We investigate the effect of pseudo-dynamic source models on the inter-frequency correlation of ground motions by simulating a number of ground motion waveforms for the 1994 Northridge, California, earthquake, using the Southern California Earthquake Center (SCEC) BroadBand Platform (BBP). We find that the cross-correlation between earthquake source parameters in pseudo-dynamic source models significantly affects the inter-frequency correlation of ground motions in the frequency around 0.5 Hz while its effect is not visible in the other frequency ranges. Our understanding of the effects of earthquake sources on the characteristics of near-source ground motions, particularly the inter-frequency correlation, may help to develop advanced physics-based ground motion simulation methods for advanced seismic hazard and risk assessments.
Suggested Reviewers:	Arben Pitarka LLNL pitarka1@llnl.gov Expertise in the field
	Hiroe Miyake ERI, Japan hiroe@eri.u-tokyo.ac.jp Expertise in the field
	Fabrice Cotton GFZ, Germany fcotton@gfz-potsdam.de

	Robert Graves USGS rwgraves22@gmail.com Expertise in the field
	Kim Olsen SDSU kbolsen@mail.sdsu.edu Expertise in the field
Opposed Reviewers:	

Sensitivity Analysis of the Inter-frequency Correlation of Synthetic Ground Motions to Pseudo-dynamic Source Models

Seok Goo Song[1], Mathieu Causse[2], and Jeff Bayless[3]

[1]Earthquake Research Center, Korea Institute of Geoscience and Mineral Resources (KIGAM), Daejeon, Republic of Korea

[2]Univ. Grenoble Alpes, Univ. Savoie Mont Blanc, CNRS, IRD, IFSTTAR, Univ. Gustave Eiffel, ISTerre, Grenoble, France

[3]AECOM, Los Angeles, USA

CORRESPONDING AUTHOR

Seok Goo Song

Address: 124 Gwahang-no, Yuseong-gu, Daejeon 34132, Republic of Korea

Tel: +82-(0)42-868-3296

Email: sgsong@kigam.re.kr

ABSTRACT

Given the deficiency of recorded strong ground motion data, it is important to understand the effects of earthquake rupture processes on near-source ground motion characteristics and to develop physics-based ground motion simulation methods for advanced seismic hazard assessments. Recently, the inter-frequency correlation of ground motions has become an important element of ground motion predictions. We investigate the effect of pseudo-dynamic source models on the inter-frequency correlation of ground motions by simulating a number of ground motion waveforms for the 1994 Northridge, California, earthquake, using the Southern California Earthquake Center (SCEC) BroadBand Platform (BBP). We find that the cross-correlation between earthquake source parameters in pseudo-dynamic source models significantly affects the inter-frequency correlation of ground motions in the frequency around 0.5 Hz while its effect is not visible in the other frequency ranges. Our understanding of the effects of earthquake sources on the characteristics of near-source ground motions, particularly the inter-frequency correlation, may help to develop advanced physics-based ground motion simulation methods for advanced seismic hazard and risk assessments.

INTRODUCTION

Ground motion prediction is an important element of the assessment of seismic hazards. In particular, for advanced seismic hazard assessment endeavors, it is important to understand the near-source ground motion characteristics of large events. Empirical ground motion prediction equations (GMPEs) have been used extensively to predict ground motion intensity measures such as the peak ground acceleration (PGA) and pseudo-spectral acceleration (PSA) (e.g., Abrahamson et al., 2008). However, although ground motions have been recorded worldwide, the quantity of recorded strong ground motions is insufficient to investigate the near-source characteristics, i.e., the intensity and variability of ground motions near earthquake fault rupture (Chiou et al., 2008). Recently, physics-based ground motion simulation approaches, including both dynamic and pseudo-dynamic earthquake rupture models, have become more popular for evaluating the near-source ground motion characteristics such as the effect of rupture directivity and fault complexity (e.g., roughness), given the availability of advanced numerical modeling schemes and rapidly growing high-performance computing capabilities (Olsen et al., 2009; Graves et al., 2011; Shi and Day, 2013).

GMPEs predict both the mean and the standard deviation of ground motion intensity measures such as PGA and PSA, given a set of explanatory seismological parameters (magnitude, distance, site conditions, etc.). Recently, several research groups pioneered a method to investigate the inter-frequency (or inter-period) correlation characteristics of ground motions by analyzing recorded ground motion data (Baker and Cornell, 2006; Baker and Jayaram, 2008; Stafford, 2017; Bayless and Abrahamson, 2019a). The inter-frequency correlation characterizes the relative width (in the frequency domain) of the extrema in a ground motion spectrum. The widths of the peaks and troughs in ground motion spectra are significant in assessments

58 involving simulated ground motions because the variability in dynamic response analyses can be
59 underestimated if simulated ground motions have an excessively low correlation (Bayless and
60 Abrahamson, 2018).

61 It would be meaningful to investigate whether physics-based ground motion simulation
62 models can produce the inter-frequency correlation of ground motions, consistent with empirical
63 correlation models, obtained by analyzing recorded ground motion data. There have been several
64 attempts to understand how well the physics-based ground motion simulation models reproduce
65 the mean and the standard deviation of ground motion intensity measures, produced by empirical
66 GMPEs (Cotton et al., 2013; Causse and Song, 2015; Imtiaz et al., 2015; Vyas et al., 2016;
67 Crempien and Archuleta, 2017; Moschetti et al., 2017; Wirth et al., 2017). Recently, Wang et al.
68 (2019) implemented an inter-frequency correlation model obtained by analyzing recorded ground
69 motion data in their physics-based broadband ground motion simulation platform. In other
70 words, they developed a post-processing method for their synthetic ground motion waveforms to
71 mimic the inter-frequency correlation structure observed in the empirical model. However, we
72 think that this study is a first attempt to understand the direct link between physics-based ground
73 motion simulation models and the inter-frequency correlation of ground motions.

74 In this study, we adopted the pseudo-dynamic source modeling method, proposed by
75 Song et al. (2014) and Song (2016), for physics-based ground motion simulations, which is
76 implemented at the SCEC BBP. Pseudo-dynamic source modeling approaches maintain the
77 computational efficiency of kinematic source modeling methods but emulate the essential
78 physics of earthquake rupture dynamics by statistically analyzing a number of dynamic rupture
79 models (Guatteri et al., 2004; Graves and Pitarka, 2010; Schmedes et al., 2013; Song et al.,
80 2014). Fayjaloun et al. (2019) and Park et al. (2020) successfully investigated the effect of the

pseudo-dynamic source models, developed by Song et al. (2014) and Song (2016), on the mean and the standard deviation of ground motions. In this study, we investigated the effect of the pseudo-dynamic source models on the inter-frequency correlation of ground motions. We first performed a series of ground motion simulations for the 1994 Northridge, California, earthquake, using various sets of pseudo-dynamic source models. Then we investigated the sensitivity of the inter-frequency correlation of the simulated ground motions to those pseudo-dynamic source models.

GROUND MOTION SIMULATION

For this research, we adopted the broadband platform (BBP) developed by the Southern California Earthquake Center (SCEC) for synthetic ground motion simulations (see Data and Resources). Multiple research groups, including both earthquake scientists and engineers, have been involved in the SCEC BBP project (Goulet et al., 2015; Maechling et al., 2015). The BBP has been thoroughly validated against both actual ground motions recorded during past earthquakes and empirical GMPEs (Dreger et al., 2015; Goulet et al., 2015). The latest version of the BBP is released regularly; here, we used V. 16.5, which was released in May 2016. Multiple modeling schemes are provided in the platform; we chose the Song method, which uses pseudo-dynamic source models, based on the 1-point and 2-point statistics of earthquake source parameters (Song et al., 2014; Song, 2016). The Song method adopts the Graves and Pitarka (GP) method (Graves and Pitarka, 2010) for the simulation of high-frequency (> 1 Hz) ground motions as well as the low-frequency (< 1 Hz) seismic wave propagation. The GP method adopts the Green's function computation method developed by Zhu and Rivera (2002), given a 1-dimensional velocity model. In this study, we primarily aimed to investigate the inter-frequency

104 correlation of ground motions in the low-frequency range, i.e., between 0.1 and 1.0 Hz. Thus, we
105 expect that the inter-frequency correlation is mainly affected by the pseudo-dynamic source
106 models, implemented in ground motion simulations.

107 The SCEC BBP performed two types of validation (Goulet et al., 2015). The first
108 validation (Part A) was against ground motion data recorded during past earthquakes in North
109 America and Japan. The second (Part B) was against empirical GMPEs. Among the Part A
110 validation events, we chose the 1994 Northridge, California, earthquake for our study. Detailed
111 information about the fault plane geometry of the event is given in Table 1 and Figure 1. The
112 Northridge event occurred in a highly populated area and produced well-recorded ground
113 motions, as shown in Figure 1. For the details of the event simulation, we followed the procedure
114 established by the SCEC BBP group (Goulet et al., 2015).

115 Given the fault geometry defined in Table 1, we prepared three sets of pseudo-dynamic
116 rupture models for our sensitivity test, as summarized in Table 2. Furthermore, we employed the
117 input source statistics models proposed by Song (2016), which are also summarized in Table 3.
118 The basic set (Test Set I) in Table 2 is composed of two groups of pseudo-dynamic source
119 models. One group contains correlated source models, while the other contains uncorrelated
120 source models. The core element in the pseudo-dynamic source models proposed by Song et al.
121 (2014) is the cross-correlation structure coupling the earthquake source parameters, such as the
122 slip, rupture velocity, and peak slip velocity. For the group of uncorrelated source models, we
123 simulated the pseudo-dynamic source models without a cross-correlation structure, as visualized
124 in Figure 2. Several studies have been performed to understand the effects of the cross-
125 correlation structure on near-source ground motions, particularly the mean and the standard

126 deviation of ground motion intensity measures such as the peak ground velocity (PGV) and PGA
127 (Fayjaloun et al., 2019; Park et al., 2020).

128 However, whereas the authors of these studies perturbed each cross-correlation
129 component individually for their sensitivity analysis, we focused on two cases, i.e., full cross-
130 correlation (correlated) and no cross-correlation (uncorrelated) between the earthquake source
131 parameters, as shown in Figure 2. For Test Set I in Table 2, we simulated 100 pseudo-dynamic
132 source models, i.e., 50 correlated and 50 uncorrelated source models. Figure 3 shows the first
133 three source models among the 50 models in the group of correlated source models, while Figure
134 4 shows the first three for the group of uncorrelated source models. In the correlated source
135 models, the source parameters (such as the slip, rupture velocity, and peak slip velocity) are
136 coupled together according to the cross-correlation structure in Figure 2a. Since the pseudo-
137 dynamic source models are obtained by stochastic modeling, based on the covariance matrix
138 constructed by the input source statistics models (Song et al., 2014), each source model exhibits
139 unique randomness; nevertheless, we can observe correlations between the source parameters in
140 Figure 3. In contrast, the distributions of the source parameters within the models depicted in
141 Figure 4 display heterogeneity, controlled by the diagonal elements of Figure 2b, but no coupling
142 between the source parameters is expected.

143 We also prepared two additional sets of pseudo-dynamic source models, i.e., Test Sets II
144 and III in Table 2, for our sensitivity analysis. In Test Set II, we randomly perturbed the
145 hypocenter of each source model. In the Part A validation, following Goulet et al. (2015), the
146 hypocenter was fixed since the validation was performed for real past events. We adopted the
147 same strategy for Test Set I. However, the hypocenter location may significantly affect the near-
148 source ground motion characteristics. Therefore, since we aimed to investigate the sensitivity of

149 ground motions to various pseudo-dynamic source models rather than to validate our pseudo-
150 dynamic source models against recorded ground motion data, we decided to test random
151 hypocenter models in Test Set II as well.

152 In Test Set III, we perturbed the stress drop by increasing or decreasing the rupture
153 dimension while holding the seismic moment constant. Since the stress drop directly affects the
154 corner frequency and hence the shape of the Fourier amplitude spectrum (e.g., Causse and Song,
155 2015), the stress drop may also affect the inter-frequency correlation characteristics of ground
156 motions. The static stress drop is proportional to the ratio of the mean slip to the characteristic
157 rupture dimension ($\tilde{L}$), as given in the equation below (Kanamori and Anderson, 1975):

158 $$\Delta\tau \approx \frac{\mu_{slip}}{\tilde{L}}. \quad (1)$$

159 Models with larger stress drops were obtained by decreasing both the rupture length and the
160 width by 30%, while models with smaller stress drops were obtained by increasing both the
161 rupture length and the width by 30%. The input source statistics for each model are presented in
162 Table 3. Figures 5 and 6 show one example each of the simulated pseudo-dynamic source
163 models with larger and smaller stress drops, respectively. In Test Set III, there are 300 pseudo-
164 dynamic source models, i.e., 150 correlated and 150 uncorrelated models, as indicated in Table
165 2. The 150 correlated source models contain 50 models with larger stress drops and 50 with
166 smaller stress drops in addition to the 50 correlated source models from Test Set I.

167 Using the SCEC BBP (V. 16.5), we simulated three-component ground motion
168 waveforms at the 133 stations illustrated in Figure 1 for each pseudo-dynamic source model. The
169 Song method adopts a hybrid approach, i.e., pseudo-dynamic low-frequency (< 1 Hz; Song,
170 2016) and stochastic high-frequency (> 1 Hz; Graves and Pitarka, 2010) modeling schemes. For
171 a systematic sensitivity analysis of the simulated ground motions with a single representative

metric for the ground motion intensity measures, we adopted the effective amplitude spectrum (EAS), computed with two horizontal-component ground motions as (Bayless and Abrahamson, 2018)

$$EAS(f) = \sqrt{\frac{1}{2}[FAS_{HC1}(f)^2 + FAS_{HC2}(f)^2]}, \quad (2)$$

where FAS_{HC1} and FAS_{HC2} are the Fourier amplitude spectra of the two orthogonal horizontal components of the three-component waveforms and f is the frequency in Hz. The EAS is independent of the orientation of the instrument. Using the average power of the two horizontal components (Eq. 2) leads to an amplitude spectrum that is compatible with the application of random vibration theory to convert the Fourier spectra into response spectra. The EAS is smoothed using the $\log_{10}$-scale smoothing window of Konno and Ohmachi (1998) with the smoothing parameters described by Kottke et al. (2018).

Figure 7 shows examples of the EASs for the three selected stations plotted in red in Figure 1. For the near-source station (nwhp, R_{rup} = 5.4 km), the low- and high-frequency EASs do not differ considerably, but for the other two stations (gllp, R_{rup} = 21.5 km; schl, R_{rup} = 40.4 km), the two frequency bands, i.e., the low-frequency (< 1 Hz) and high-frequency (> 1 Hz) bands, show distinctive EAS patterns. Since we used the abovementioned hybrid approach, the low- and high-frequency ground motions may not behave consistently for all rupture scenarios and station locations. This issue may need to be investigated further for all hybrid ground motion simulation methods offered by the SCEC BBP. In this study, we aimed predominantly to analyze low-frequency (< 1 Hz) ground motions, which are affected by the cross-correlation structure of the input pseudo-dynamic source models, for the sensitivity analysis of inter-frequency correlations. We also added the mean and the standard deviation values predicted by the

empirical model (Bayless and Abrahamson, 2019b) to the figure for comparison purposes. The empirical model used in the study will be discussed in more details in the next section.

CORRELATION ANALYSIS

Bayless and Abrahamson (2019ab) developed both the inter-frequency correlation model and the GMPE using the Next Generation Attenuation-West2 (NGA-West2; Ancheta et al, 2014) database, which includes shallow crustal earthquakes in active tectonic regions. Their models adopt the effective amplitude spectrum (EAS), which is based on the Fourier Amplitude Spectra (FAS), in equation (2) as ground motion intensity measure. Bayless and Abrahamson (2019b) clearly described the benefit of using the EAS than response spectra in their paper. We adopted their EAS based GMPE and inter-frequency correlation model to compare with our synthetics since the Fourier spectra are more closely related to the physics-based simulations. Their empirical models also provide individual residual components for more detailed comparison. Residuals from empirical GMPEs are typically partitioned into between-event residual (δB), and within-event residuals (δW), following the notation of Al Atik et al., (2010). For large numbers of recordings per earthquake, the between-event residual is approximately the average difference in logarithmic-space between the observed Intensity Measure (IM) from a specific earthquake and the IM predicted by the GMPE. The within-event residual (δW) is the difference between the IM at a specific site for a given earthquake and the median IM predicted by the GMPE plus δB. By accounting for repeatable site effects, δW can further be partitioned into a site-to-site residual (δS2S) and the within-site residual (δWS). More detailed description about the residual partitioning, including the mathematical description of the inter-frequency correlation (both between- and within-event), is provided in Bayless and Abrahamson (2018).

Figure 8 shows the mean residuals on a natural logarithmic scale between the simulated EASs and the EASs predicted by the empirical GMPE (Bayless and Abrahamson, 2019b) for both the correlated and the uncorrelated models in Test Set I. We observed that the mean of the synthetic EASs underpredicts the mean of the GMPE at the low frequency, while the mean of the former overpredicts that of the latter at the high frequency. At the low frequency, the correlated models produce slightly higher EASs, as was also observed in previous studies (Song et al., 2014; Song, 2016; Fayjaloun et al., 2019; Park et al., 2020). Since we compared synthetic ground motions produced by simulating a specific earthquake, i.e., the Northridge event, and because we constructed the mean of the GMPE by using recorded ground motions from various events worldwide, the bias we observe in Figure 8 may be reasonable and may be considered part of the between-event variability (Al Atik et al., 2010). In addition, we aimed to investigate mainly the relative sensitivity of the inter-frequency correlation of our synthetic ground motions in this study rather than to reproduce the absolute level of ground motion intensities constrained by empirical GMPEs.

The variability (e.g., standard deviation) of ground motions is an important consideration in ground motion prediction (Abrahamson et al., 2008; Cotton et al., 2013; Causse and Song, 2015; Imtiaz et al., 2015; Vyas et al., 2016; Crempien and Archuleta, 2017; Withers et al., 2019ab). Figure 9 shows the standard deviations for both the between-event and the within-event components of the EAS residuals from the three sets of model tests. The between-event term is calculated from various realizations of the source within each test set. First, little difference is noted between the ground motions obtained from the correlated and uncorrelated pseudo-dynamic source models. In other words, the cross-correlations between the earthquake source parameters in Figure 2 do not significantly affect both the between-event and the within-event

240 standard deviations in our simulations. Crempien and Archuleta (2017) found that the longer
241 correlation (i.e., autocorrelation) of earthquake slip increases both the between- and within-event
242 standard deviations of ground motions. The cross-correlation of pseudo-dynamic source models
243 does not seem to play a significant role in determining the standard deviation in our simulations,
244 but may need to be further investigated in subsequent studies to confirm its behavior.
245 Note that the between-event standard deviation for Test Set II (random hypocenter) is
246 much larger than that for the other two test sets. Since Test Set II introduces randomly located
247 hypocenters, this discrepancy implies that randomizing the hypocenter has a greater effect on the
248 between-event variability than does the stress drop perturbation. It is also noticeable that the
249 random hypocenter models reduce the within-event standard deviation significantly as shown in
250 Figure 9b. We also compared them with the standard deviations from the empirical GMPE
251 (Bayless and Abrahamson, 2019b) as indicated in black lines. Regarding the between-event
252 standard deviation, the empirical model is consistent with the synthetic ground motions with the
253 random hypocenter models. Regarding the within-event standard deviation, in general synthetic
254 ground motions produce larger values. For the random hypocenter model in Figure 9b, the
255 difference is minimized. However, if we consider only the within-site (δWS) standard deviation
256 without the between-site (δS2S) term since the site effect was not included in our simulations,
257 the synthetics still produce larger standard deviations. Note that we restricted our analysis to the
258 low frequency below 1 Hz although we show the results up to 10 Hz for reference in the figure.
259 The main goal of this study was to investigate the effect of cross-correlations between
260 earthquake source parameters, such as the slip, rupture velocity, and peak slip velocity, in
261 pseudo-dynamic source models on the inter-frequency correlation of ground motions. Figure 10
262 shows the between-event inter-frequency correlations of the synthetic EASs for the three sets of

model tests in the low-frequency band (0.1 – 1.0 Hz) with those from an empirical model (Bayless and Abrahamson, 2019a). Interestingly, the between-event inter-frequency correlations for the fixed-hypocenter models decay much faster than those for the empirical model as the frequency deviates from the reference frequencies (0.2, 0.3, 0.4, 0.5, and 1.0 Hz), while the random hypocenter models produce inter-frequency correlations that are compatible with those from the empirical model. More remarkably, we found distinctive features between the correlated and uncorrelated models at approximately 0.5 Hz (2 s) when the reference frequencies were 0.4 Hz (Test Set II) or 0.5 Hz (Test Sets I and III): the correlated source models (in red) produced higher inter-frequency correlations than the uncorrelated source models (in blue) for all three test sets at approximately 0.5 Hz, although the difference was not significant at the other reference frequencies. In this analysis, we focus more on the correlation near each reference frequency, i.e., initial decay pattern from each reference frequency. Thus we show correlations only between 0.6 and 1.0 in Figure 10. The correlation at the far distance in the spectral domain may need to be analyzed further in subsequent studies. This observation, however, may imply that the cross-correlation between earthquake source parameters in pseudo-dynamic source models affects the initial decay pattern of the inter-frequency correlation of ground motions in a certain frequency range, as depicted with solid red and blue traces in Figure 10.

Within-event residuals represent the variability in the path effects and directivity effects for a given event at various stations. Figure 11 indicates that the inter-frequency correlations of simulated ground motions systematically exceed those of the empirical model. And we do not observe significant differences between correlated and uncorrelated pseudo-dynamic source models. It is not clear yet why the synthetic ground motions produce broader inter-frequency correlation structure than the empirical model. Based on Bayless and Abrahamson (2018), the

fully stochastic ground motion simulation method (e.g., Atkinson and Assatourians, 2015) produce the within-event inter-frequency correlations compatible with the empirical model (figure 10b of Bayless and Abrahamson (2018)) while the physics-based ground motion simulation methods produce the correlations, which are broader than the empirical model (figures 11b, 12b, 13b and 14b of Bayless and Abrahamson (2018)). It is still puzzling why the physics-based methods, which more explicitly handle wave propagation effects such as directivity, produce the within-event correlations inconsistent with the empirical model. Although we aim to focus more on the effect of earthquake source on the inter-frequency correlations, i.e., between-event, the inconsistency observed in the within-event correlation may need to be investigated further in subsequent studies.

DISCUSSION

In Figure 10, the cross-correlation in the pseudo-dynamic source models affects the between-event inter-frequency correlation of ground motions in a specific frequency range, i.e., approximately 0.5 Hz. However, it is not yet clear why the frequency range centered at approximately 0.5 Hz is strongly affected by the cross-correlation of pseudo-dynamic source models for the Northridge, California, earthquake. It is also surprising that there are almost no differences in the other frequency ranges. This phenomenon may be linked to the magnitude of the simulated event or the event type. The reason may become clearer if we perform more sensitivity analyses over a wide range of magnitudes and event types in subsequent studies. Moreover, the number and positions of stations used in the analyses may also affect the outcomes. Test Sets II and III clearly indicate that the inter-frequency correlation can be affected by randomized hypocenter locations and stress drop perturbations more significantly than by

input source statistics perturbations, as shown in Table 3. Hence, we need to carefully consider these source parameters, such as the hypocenter and stress drop, even when we focus on investigating the effects of the detailed input source statistics in Table 3 on the characteristics of ground motions. Finally, our sensitivity analyses clearly indicate that the cross-correlation structure in the pseudo-dynamic source models affects the inter-frequency correlation more significantly than the standard deviation of the ground motions. We may also employ the empirical inter-frequency correlation model (Bayless and Abrahamson, 2019a) to constrain the cross-correlation structure of pseudo-dynamic source models.

There have been several attempts to investigate the effects of pseudo-dynamic source models on the mean and standard deviation of ground motions (Song et al., 2014; Song, 2016; Fayjaloun et al., 2019; Park et al., 2020). However, this study is the first attempt to investigate the effect of pseudo-dynamic source models on the inter-frequency correlation of ground motions. Interestingly, we found that the cross-correlation structure, which is a core element of the pseudo-dynamic source modeling approach proposed by Song et al. (2014), may significantly affect the inter-frequency correlation of ground motions, at least in a specific frequency range. Nevertheless, we may need more comprehensive sensitivity analyses to understand the link between pseudo-dynamic source models and the inter-frequency correlation of ground motions in greater detail. However, we believe that this pilot study already shows the potential of physics-based ground motion simulation methods provided by the SCEC BBP for studying the inter-frequency correlation characteristics of ground motions.

CONCLUSIONS

In this study, we investigated the effect of pseudo-dynamic source models, particularly their cross-correlation structure between earthquake source parameters, on the inter-frequency correlation of ground motions by simulating a number of ground motions for the 1994 Northridge, California, earthquake using the SCEC BBP. We found that the cross-correlation of pseudo-dynamic source models significantly affects the between-event inter-frequency correlation at a specific frequency range (at approximately 0.5 Hz), while the effect on the standard deviation of ground motions is not significant. It is important to understand the inter-frequency correlation characteristics of ground motions in ground motion predictions. This type of study may help to understand the relation between physics-based earthquake source models and the inter-frequency correlation of ground motions and consequently to develop physics-based ground motion simulation methods for advanced seismic hazard and risk assessments.

DATA AND RESOURCES

We simulated synthetic 3-component ground motion waveforms using the SCEC BBP (V. 16.5), which is available online (http://scec.usc.edu/scecpedia/Broadband_Platform, last accessed April 2020). The stand-alone version of the pseudo-dynamic rupture model generator, used in the study, is also available online (http://www.github.com/sgsong1017/SongRMG, last accessed July 2020).

ACKNOWLEDGMENTS

We appreciate the editor's and three anonymous reviewers' comments, which helped to improve the paper significantly. We would like to thank F. Silva, P. Maechling, C. Goulet, and R.W. Graves for their kind technical and scientific support regarding the SCEC BBP. This study was

354 supported by a See-At Project funded by the Korea Meteorological Administration (KMA)
355 (KMI2018-01810) and by a Basic Research Project of the Korea Institute of Geoscience and
356 Mineral Resources (KIGAM), funded by the Ministry of Science and ICT (MSIT, Korea)
357 (GP2020-027).

REFERENCES

Abrahamson, N., G. Atkinson, D. Boore, Y. Bozorgnia, K. Campbell, B. Chiou, I. M. Idriss, W. Silva, and R. Youngs (2008). Comparisons of the NGA ground-motion relations, *Earthquake Spectra* **24** 45-66.

Al Atik, L., N. Abrahamson, J. J. Bommer, F. Scherbaum, F. Cotton, and N. Kuehn (2010). The variability of ground-motion prediction models and its components, *Seismol. Res. Lett.* **81** 794-801.

Ancheta, T. D., R. B. Darragh, J. P. Stewart, E. Seyhan, W. J. Silva, B. S.-J. Chiou, K. E.Wooddell, R.W. Graves, A. R. Kottke, D. M. Boore, et al. (2014). NGA-West2 database, *Earthquake Spectra* 30, 989–1005.

Atkinson, G.M., and K. Assatourians (2015). Implementation and validation of EXSIM (A stochastic finite-fault ground-motion simulation algorithm) on the SCEC broadband platform, *Seismol. Res. Lett.* **86** 48-60.

Baker, J. W., and C. A. Cornell (2006). Correlation of response spectral values for multicomponent ground motions, *Bull. Seismol. Soc. Am.* **96** 215-227.

Baker, J. W., and N. Jayaram (2008). Correlation of spectral acceleration values from nga ground motion models, *Earthquake Spectra* **24** 299-317.

Bayless, J., and N. A. Abrahamson (2018). Evaluation of the interperiod correlation of ground‐motion simulations, *Bull. Seismol. Soc. Am.* **108** 3413-3430.

Bayless, J., and N. A. Abrahamson (2019a). An empirical model for the interfrequency correlation of epsilon for fourier amplitude spectra, *Bull. Seismol. Soc. Am.* **109** 1058-1070.

Bayless, J., and N. A. Abrahamson (2019b). Summary of the BA18 ground‐motion model for

fourier amplitude spectra for crustal earthquakes in California, *Bull. Seismol. Soc. Am.* **109** 2088-2105.

Causse, M., and S. G. Song (2015). Are stress drop and rupture velocity of earthquakes independent? Insight from observed ground motion variability, *Geophys. Res. Lett.* **42** 7383-7389.

Chiou, B., R. Darragh, N. Gregor, and W. Silva (2008). NGA project strong-motion database, *Earthquake Spectra* **24** 23-44.

Cotton, F., R. Archuleta, and M. Causse (2013). What is sigma of the stress drop?, *Seismol. Res. Lett.* **84** 42-48.

Crempien, J. G. F., and R. J. Archuleta (2017). Within-event and between-events ground motion variability from earthquake rupture scenarios, *Pure Appl. Geophys.* **174** 3451-3465.

Dreger, D. S., G. C. Beroza, S. M. Day, C. A. Goulet, T. H. Jordan, P. A. Spudich, and J. P. Stewart (2015). Validation of the SCEC broadband platform V14.3 simulation methods using pseudospectral acceleration data, *Seismol. Res. Lett.* **86** 39-47.

Fayjaloun, R., M. Causse, C. Cornou, C. Voisin, and S. G. Song (2019). Sensitivity of high-frequency ground motion to kinematic source parameters, *Pure Appl. Geophys.* doi: 10.1007/s00024-019-02195-3

Goulet, C. A., N. A. Abrahamson, P. G. Somerville, and K. E. Wooddell (2015). The SCEC broadband platform validation exercise: methodology for code validation in the context of seismic-hazard analyses, *Seismol. Res. Lett.* **86** 17-26.

Graves, R., T. H. Jordan, S. Callaghan, E. Deelman, E. Field, G. Juve, C. Kesselman, P. Maechling, G. Mehta, K. Milner, D. Okaya, P. Small, and K. Vahi (2011). Cybershake: a physics-based seismic hazard model for Southern California, *Pure Appl. Geophys.* **168**

367-381.

Graves, R. W., and A. Pitarka (2010). Broadband ground-motion simulation using a hybrid approach, *Bull. Seismol. Soc. Am.* **100** 2095-2123.

Guatteri, M., P.M. Mai, and G.C. Beroza (2004). A pseudo-dynamic approximation to dynamic rupture models for strong ground motion prediction, *Bull. Seismol. Soc. Am.* **94** 2051-2063.

Imtiaz, A., M. Causse, E. Chaljub, and F. Cotton (2015). Is ground‐motion variability distance dependent? Insight from finite‐source rupture simulations, *Bull. Seismol. Soc. Am.* **105** 950-962.

Kanamori, H., and D. L. Anderson (1975). Theoretical basis of some empirical relations in seismology, *Bull. Seismol. Soc. Am.* **65** 1073-1095.

Konno, K., and T. Ohmachi (1998). Ground-motion characteristics estimated from spectral ratio between horizontal and vertical components of microtremor, *Bull. Seismol. Soc. Am.* **88** 228-241.

Kottke, A., E. Rathje, D. M. Boore, E. Thompson, J. Hollenback, N. Kuehn, C. A. Goulet, N. A. Abrahamson, Y. Bozorgnia, and A. D. Kiureghian (2018). *Selection of random vibration procedures for the NGA east project, PEER Rept. No. 2018/05*. Pacific Earthquake Engineering Research Center, University of California, Berkeley, California.

Maechling, P. J., F. Silva, S. Callaghan, and T. H. Jordan (2015). SCEC broadband platform: system architecture and software implementation, *Seismol. Res. Lett.* **86** 27-38.

Moschetti, M. P., S. Hartzell, L. Ramírez‐Guzmán, A. D. Frankel, S. J. Angster, and W. J. Stephenson (2017). 3D ground-motion simulations of Mw 7 earthquakes on the salt lake city segment of the wasatch fault zone: variability of long-period ($T \geq 1$ s) ground

motions and sensitivity to kinematic rupture parameters, *Bull. Seismol. Soc. Am.* **107** 1704-1723.

Olsen, K. B., S. M. Day, L. A. Dalguer, J. Mayhew, Y. Cui, J. Zhu, V. M. Cruz-Atienza, D. Roten, P. Maechling, T. H. Jordan, D. Okaya, and A. Chourasia (2009). ShakeOut-D: ground motion estimates using an ensemble of large earthquakes on the southern San Andreas fault with spontaneous rupture propagation, *Geophys. Res. Lett.* **36** L04303.

Park, D., S. G. Song, and J. Rhie (2020). Sensitivity analysis of near-source ground motions to pseudo-dynamic source models derived with 1-point and 2-point statistics of earthquake source parameters, *J. Seismol.* doi: 10.1007/s10950-020-09905-8

Schmedes, J., R. J. Archuleta, and D. Lavallée (2013). A kinematic rupture model generator incorporating spatial interdependency of earthquake source parameters, *Geophys. J. Int.* **192** 1116-1131.

Shi, Z., and S. M. Day (2013). Rupture dynamics and ground motion from 3-D rough-fault simulations, *J. Geophys. Res. Solid Earth* **118** 1122-1141.

Song, S. G. (2016). Developing a generalized pseudo-dynamic source model ofMw6.5–7.0 to simulate strong ground motions, *Geophys. J. Int.* **204** 1254-1265.

Song, S. G., L. A. Dalguer, and P. M. Mai (2014). Pseudo-dynamic source modelling with 1-point and 2-point statistics of earthquake source parameters, *Geophys. J. Int.* **196** 1770-1786.

Stafford, P. J. (2017). Interfrequency correlations among fourier spectral ordinates and implications for stochastic ground‐motion simulation, *Bull. Seismol. Soc. Am.* **107** 2774-2791.

Vyas, J. C., P. M. Mai, and M. Galis (2016). Distance and azimuthal dependence of ground‐

motion variability for unilateral strike‐slip ruptures, *Bull. Seismol. Soc. Am.* **106** 1584-1599.

Wang, N., R. Takedatsu, K. B. Olsen, and S. M. Day (2019). Broadband ground‐motion simulation with interfrequency correlations, *Bull. Seismol. Soc. Am.* **109** 2437-2446.

Wirth, E. A., A. D. Frankel, and J. E. Vidale (2017). Evaluating a kinematic method for generating broadband ground motions for great subduction zone earthquakes: application to the 2003 M w 8.3 Tokachi‐Oki Earthquake, *Bull. Seismol. Soc. Am.* **107** 1737-1753.

Withers, K.W., K.B. Olsen, Z. Shi, and S.M. Day (2019a). Ground motion and intra-event variability from 3-D deterministic broadband (0-7.5 Hz) simulations along a non-planar strike-slip fault, *Bull. Seismol. Soc. Am*. **109** 212-228.

Withers, K.W., K.B. Olsen, Z. Shi, and S.M. Day (2019b). Validation of deterministic broadband ground motion and variability from dynamic rupture simulations of buried thrust earthquakes, *Bull. Seismol. Soc. Am.* **109** 229-250.

Zhu, L.P., and L.A. Rivera (2002). A note on the dynamic and static discplacements from a point source in multilayered media, *Geophys. J. Int.* **148** 619-627.

FULL MAILING ADDRESS FOR EACH AUTHOR

Seok Goo Song

Earthquake Research Center, Korea Institute of Geoscience and Mineral Resources

124 Gwahang-no, Yuseong-gu, Daejeon 34132, Republic of Korea

sgsong@kigam.re.kr

(S.G. Song)

Mathieu Causse

Univ. Grenoble Alpes, Univ. Savoie Mont Blanc, CNRS, IRD, IFSTTAR, Univ. Gustave Eiffel, ISTerre

Grenoble 38000, France

mathieu.causse@univ-grenoble-alpes.fr

(M. Causse)

Jeff Bayless

AECOM

One California Plaza, 300 S Grand Avenue, Los Angeles, California 90071, USA

jeff.bayless@aecom.com

(J. Bayless)

TABLES

Table 1. Fault geometry of the Northridge earthquake

Magnitude	6.73
Strike, dip, rake	122°, 40°, 105°
Length, width	20 km, 27 km
HTop[1)]	5 km
Top center[2)] (latitude, longitude)	34.344°, -118.515°
Hypocenter (shyp[3)], dhyp[4)])	6.0 km, 19.4 km

[1)] Depth to the top of the fault plane

[2)] Geographical location of the center of the top fault plane boundary

[3)] Hypocenter location in the along-strike direction (distance from the top center of the fault plane)

[4)] Hypocenter location in the along-dip direction (distance from the top center of the fault plane)

494 **Table 2.** Three sets of model tests

	Number of pseudo-dynamic source models	Description
Test Set I (Basic)	100 (50 + 50)	- 50 correlated and 50 uncorrelated source models
Test Set II (Random hypocenter)	100 (50 + 50)	- Same as Test Set I except that the hypocenter is randomly perturbed
Test Set III (Stress drop perturbation)	300 (150 + 150)	- 150 correlated and 150 uncorrelated source models: the 150 correlated source models are composed of 50 models from Test Set I, 50 models with a larger stress drop, and 50 models with a smaller stress drop; the 150 uncorrelated source models are produced the same way

495

496 **Table 3**. Input source statistics model

	Model Parameters	Description	Basic	Larger Stress Drop	Smaller Stress Drop
1-Point Statistics	μ_{slip}	Mean slip (cm)	78.36	159.08	46.50
	μ_{V_r}	Mean rupture velocity (km/s)	3.27	3.30	3.26
	$\mu_{V_{max}}$	Mean peak slip velocity (cm/s)	114.93	158.24	97.84
	σ_{slip}	Standard deviation of slip (cm)	45.15	90.83	27.11
	σ_{V_r}	Standard deviation of rupture velocity (km/s)	1.08	1.17	1.04
	$\sigma_{V_{max}}$	Standard deviation of peak slip velocity (cm/s)	89.00	125.64	74.54
2-Point Statistics	a_x	Correlation length in the along-strike direction (km) (slip *vs.* slip, slip *vs.* V_r, slip *vs.* V_{max}, V_r *vs.* V_r, V_r *vs.* V_{max}, and V_{max} *vs.* V_{max})	$\begin{pmatrix} 3.9 & 2.7 & 2.4 \\ & 1.3 & 5.6 \\ & & 6.2 \end{pmatrix}$	$\begin{pmatrix} 3.5 & 2.6 & 1.7 \\ & 1.3 & 4.9 \\ & & 4.7 \end{pmatrix}$	$\begin{pmatrix} 4.1 & 2.7 & 2.7 \\ & 1.3 & 5.9 \\ & & 7.0 \end{pmatrix}$
	a_z	Correlation length in the along-dip direction (km) (slip *vs.* slip, slip *vs.* V_r, slip *vs.* V_{max}, V_r *vs.* V_r, V_r *vs.* V_{max}, and V_{max} *vs.* V_{max})	$\begin{pmatrix} 5.6 & 2.0 & 1.6 \\ & 3.6 & 1.4 \\ & & 1.9 \end{pmatrix}$	$\begin{pmatrix} 13.3 & 4.0 & 3.9 \\ & 4.2 & 1.9 \\ & & 2.4 \end{pmatrix}$	$\begin{pmatrix} 4.0 & 1.5 & 1.1 \\ & 3.4 & 1.3 \\ & & 1.8 \end{pmatrix}$
	ρ_{max}	Maximum correlation coefficient (slip *vs.* V_r, slip *vs.* V_{max}, and V_r *vs.* V_{max})	$\begin{pmatrix} 1 & 0.72 & 0.94 \\ & 1 & 0.64 \\ & & 1 \end{pmatrix}$	$\begin{pmatrix} 1 & 0.81 & 0.89 \\ & 1 & 0.69 \\ & & 1 \end{pmatrix}$	$\begin{pmatrix} 1 & 0.68 & 0.96 \\ & 1 & 0.62 \\ & & 1 \end{pmatrix}$

LIST OF FIGURE CAPTIONS

Figure 1. Fault geometry and station locations for the 1994 Northridge, California, earthquake. The black box indicates the ground surface projection of the fault plane; i.e., the top of the fault plane is depicted by a solid line, and the rest of the fault plane is delineated with dashed lines. Triangles show the locations of the 133 stations used in the simulation, including the three selected stations in red.

Figure 2. Input correlation model (Test Set I). (a) Correlated, (b) uncorrelated, i.e., without a cross-correlation structure.

Figure 3. Correlated pseudo-dynamic source models. The contour lines in the middle panels indicate rupture time distributions. The hypocenter is located at the bottom right corner of the rupture area.

Figure 4. Uncorrelated pseudo-dynamic source models. The contour lines in the middle panels indicate rupture time distributions. The hypocenter is located at the bottom right corner of the rupture area.

Figure 5. Pseudo-dynamic source models with a larger stress drop. (a) Correlated, (b) uncorrelated. The contour lines in the middle panels indicate rupture time distributions. The hypocenter is located at the bottom right corner of the rupture area.

Figure 6. Pseudo-dynamic source models with a smaller stress drop. (a) Correlated, (b) uncorrelated. The contour lines in the middle panels indicate rupture time distributions. The hypocenter is located at the bottom right corner of the rupture area.

Figure 7. EASs obtained from Test Set I for the three stations plotted in red in Figure 1. Fifty EAS values are plotted in cyan for each panel. The 50^{th} EAS is added in red as an example. [left] EASs obtained from the correlated pseudo-dynamic source models; [right] EASs obtained from

the uncorrelated source models. Both mean and standard deviation from the empirical GMPE model (Bayless and Abrahamson, 2019b) are presented for comparison purposes.

Figure 8. Mean residuals between the simulated EASs and those predicted by the empirical GMPE (Bayless and Abrahamson, 2018b). (a) Test Set I (basic), (b) Test Set II (random hypocenter), and (c) Test Set III (stress drop perturbation).

Figure 9. Standard deviations (tau: between-event, phi: within-event, and phi0: within-site) of the EAS residuals in (a) Test Set I (basic), (b) Test Set II (random hypocenter), and (c) Test Set III (stress drop perturbation). For the within-event standard deviation from the empirical model, both the within-event (i.e., within-site and between-site terms) and only the within-site standard deviations are presented for the comparison purposes.

Figure 10. Inter-frequency correlations (between-event) with 5 reference frequencies (0.2, 0.3, 0.4, 0.5, and 1.0 Hz) in (a) Test Set I (basic), (b) Test Set II (random hypocenter), and (c) Test Set III (stress drop perturbation).

Figure 11. Inter-frequency correlations (within-event) with 5 reference frequencies (0.2, 0.3, 0.4, 0.5, and 1.0 Hz) in (a) Test Set I (basic), (b) Test Set II (random hypocenter), and (c) Test Set III (stress drop perturbation).

FIGURES

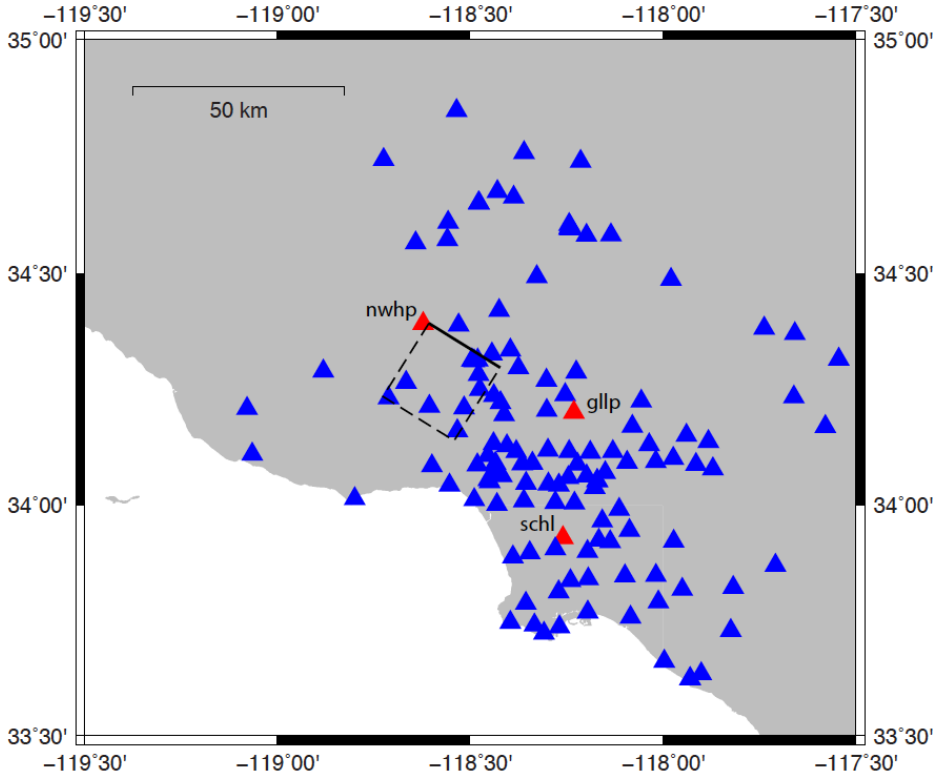

Figure 1. Fault geometry and station locations for the 1994 Northridge, California, earthquake. The black box indicates the ground surface projection of the fault plane; i.e., the top of the fault plane is depicted by a solid line, and the rest of the fault plane is delineated with dashed lines. Triangles show the locations of the 133 stations used in the simulation, including the three selected stations in red.

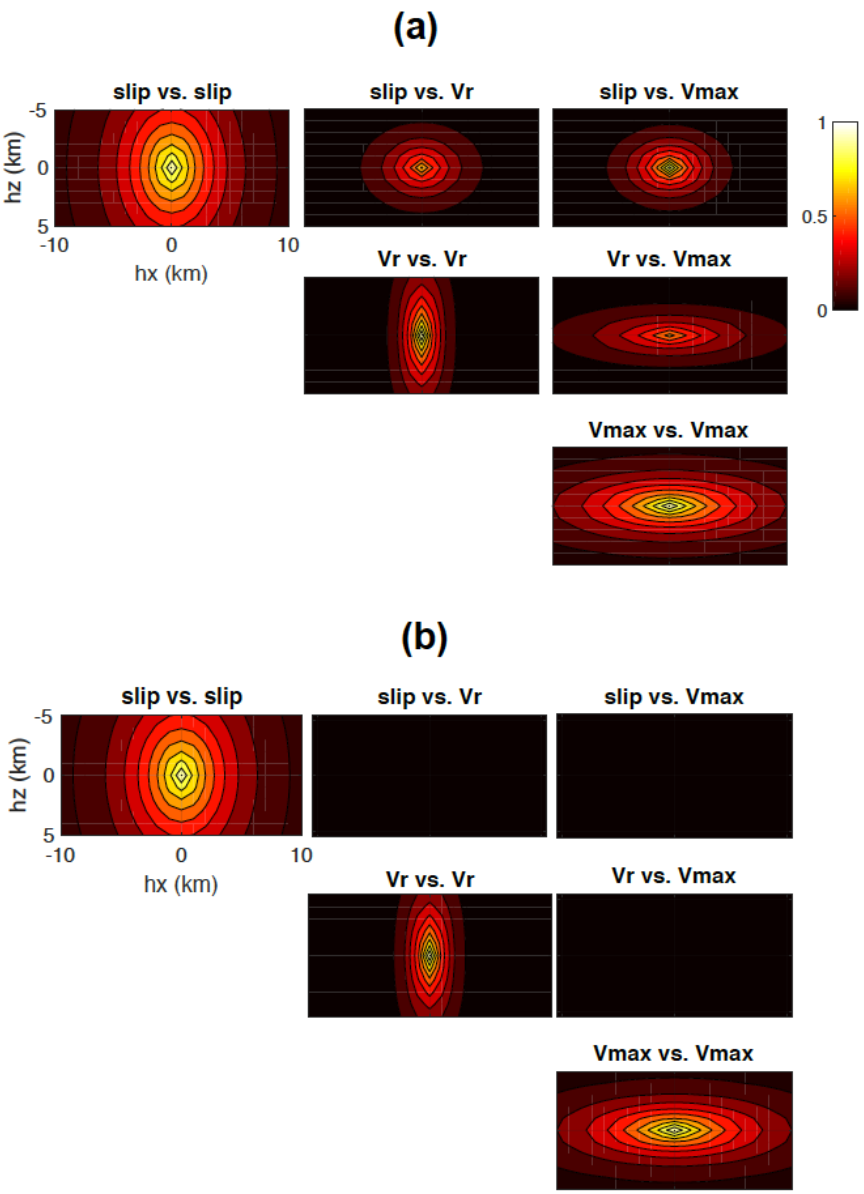

551

552 **Figure 2**. Input correlation model (Test Set I). (a) Correlated, (b) uncorrelated, i.e., without a

553 cross-correlation structure.

554

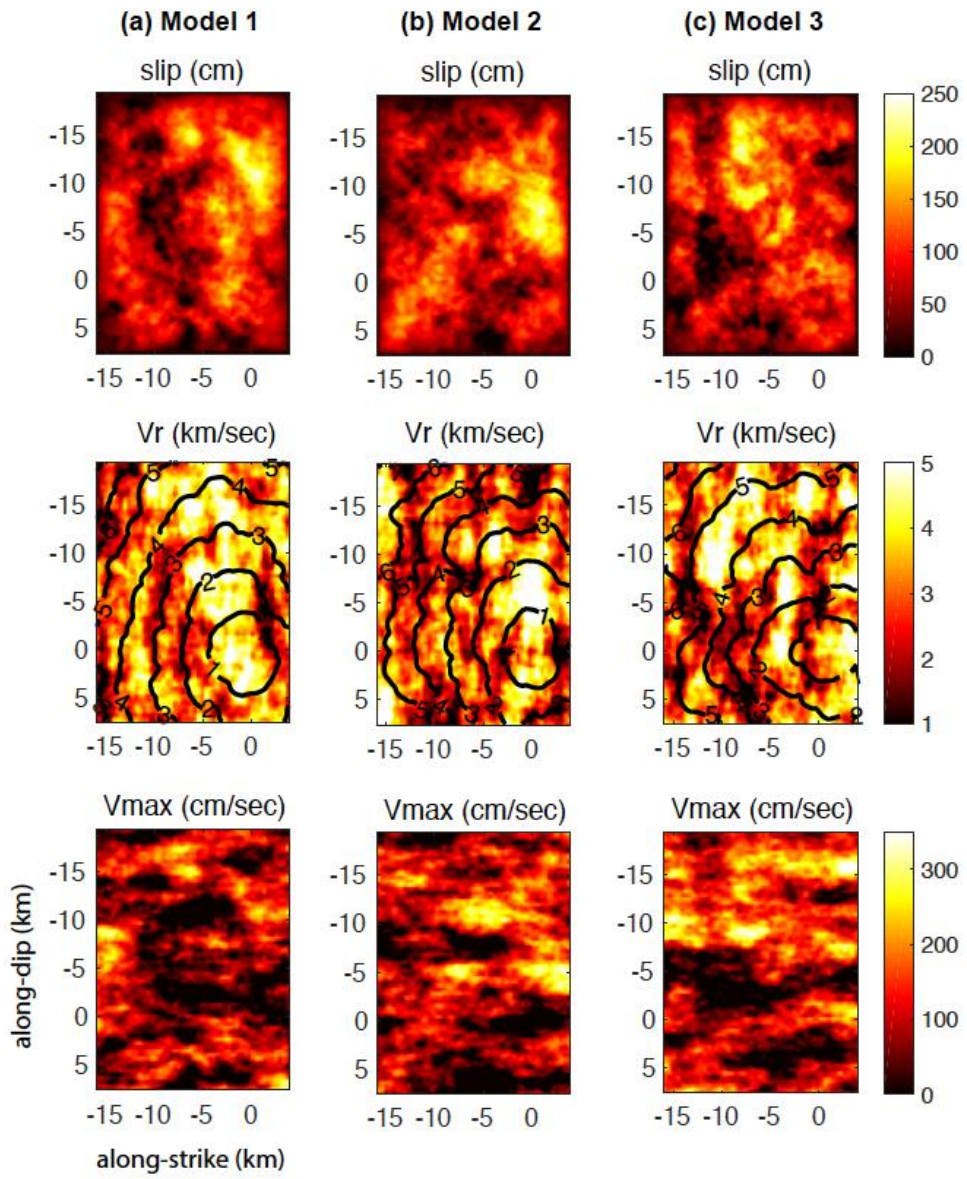

Figure 3. Correlated pseudo-dynamic source models. The contour lines in the middle panels indicate rupture time distributions. The hypocenter is located at the bottom right corner of the rupture area.

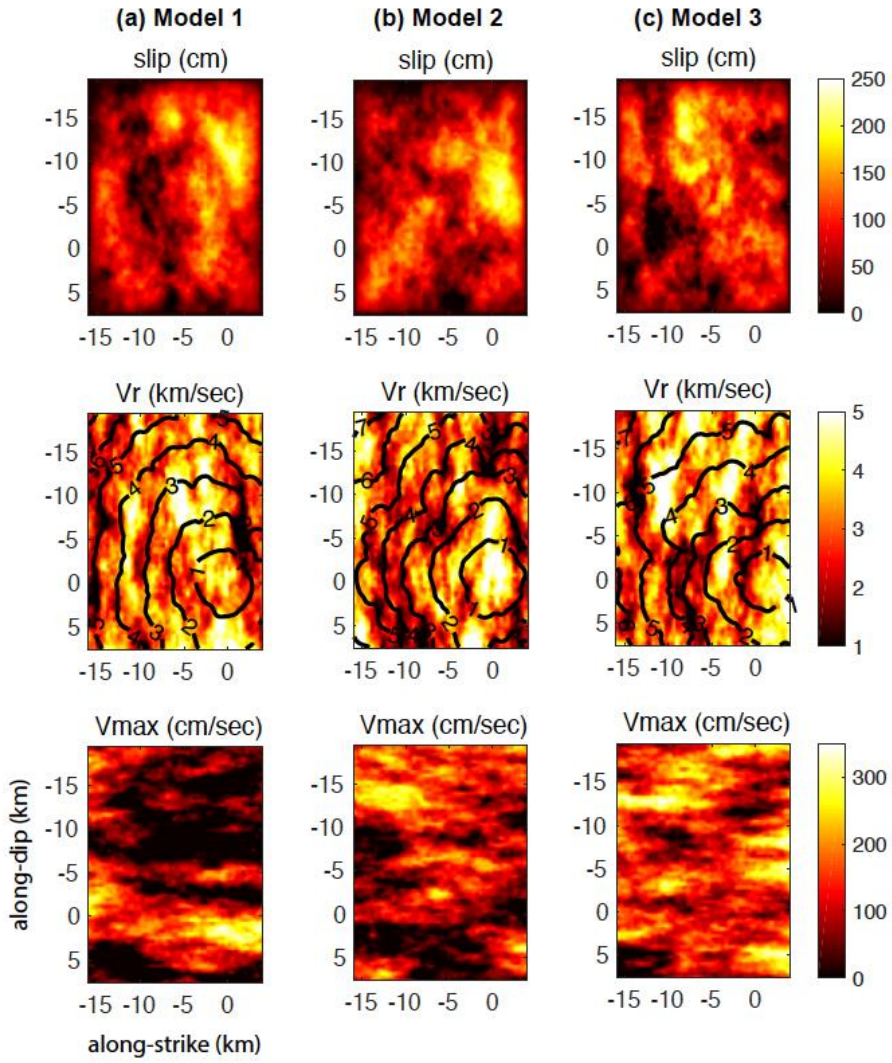

561

562 **Figure 4**. Uncorrelated pseudo-dynamic source models. The contour lines in the middle panels

563 indicate rupture time distributions. The hypocenter is located at the bottom right corner of the

564 rupture area.

565

566

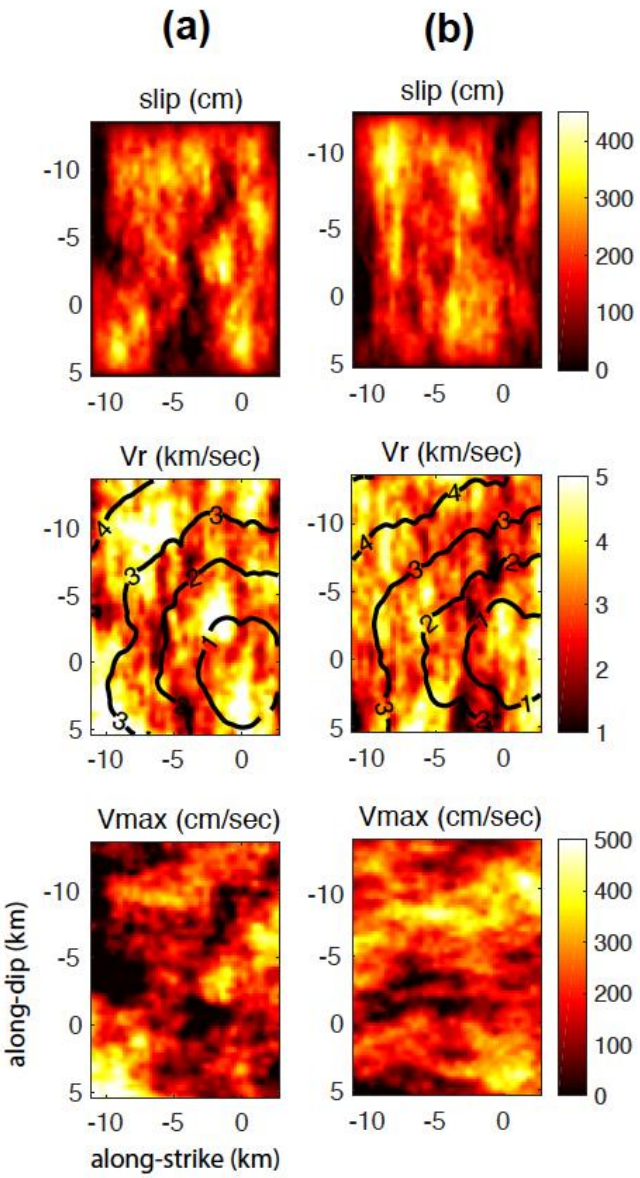

567

568 **Figure 5.** Pseudo-dynamic source models with a larger stress drop. (a) Correlated, (b)

569 uncorrelated. The contour lines in the middle panels indicate rupture time distributions. The

570 hypocenter is located at the bottom right corner of the rupture area.

571

572

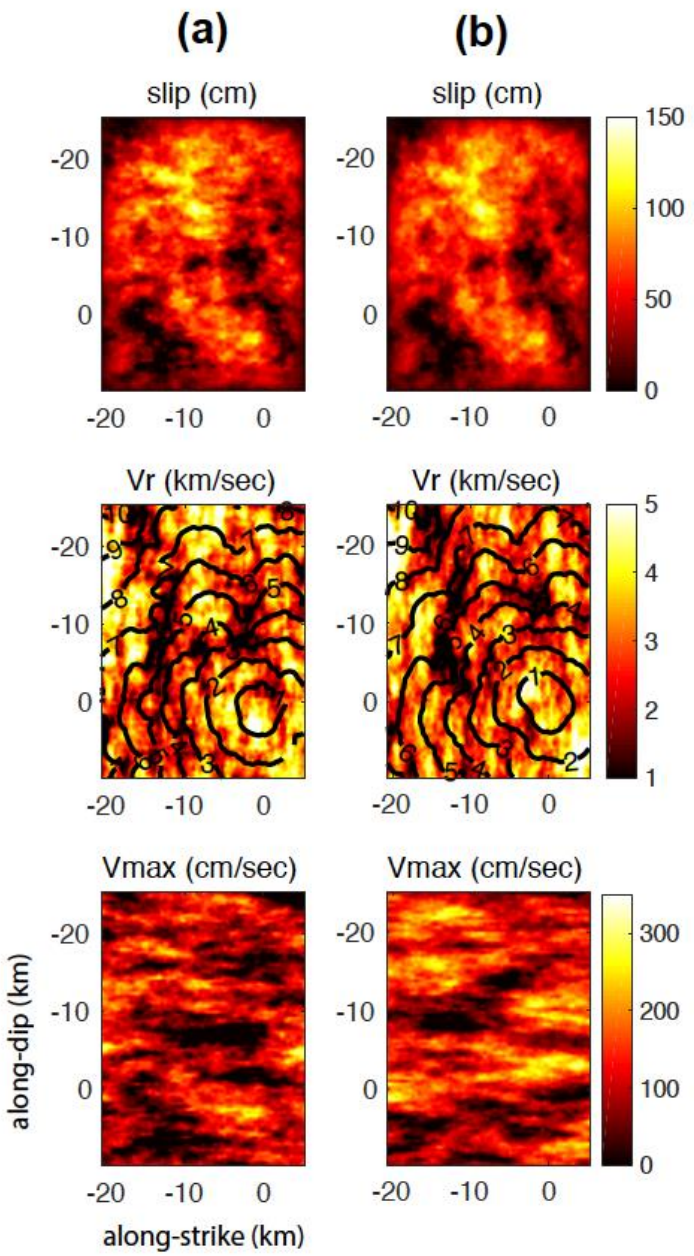

573

574 **Figure 6**. Pseudo-dynamic source models with a smaller stress drop. (a) Correlated, (b)

575 uncorrelated. The contour lines in the middle panels indicate rupture time distributions. The

576 hypocenter is located at the bottom right corner of the rupture area.

577

578

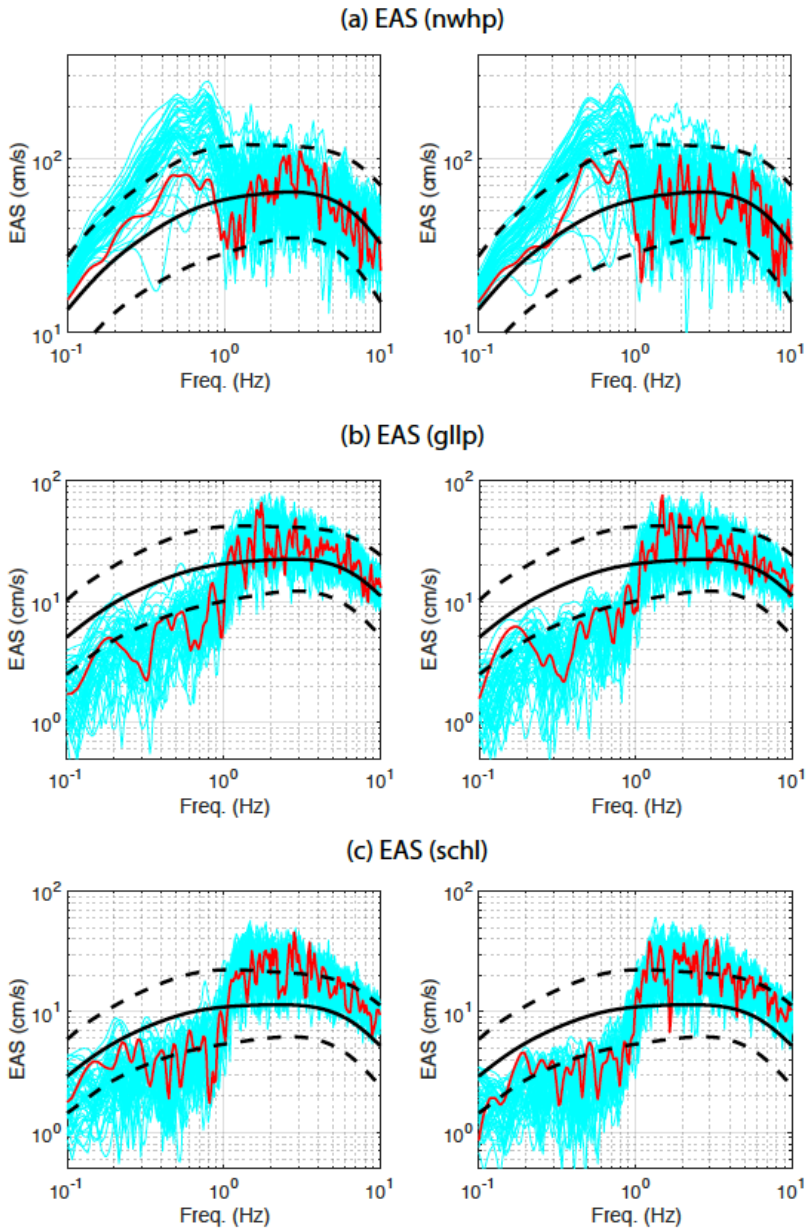

579

580 **Figure 7**. EASs obtained from Test Set I for the three stations plotted in red in Figure 1. Fifty
581 EAS values are plotted in cyan for each panel. The 50th EAS is added in red as an example. [left]
582 EASs obtained from the correlated pseudo-dynamic source models; [right] EASs obtained from
583 the uncorrelated source models. Both mean and standard deviation from the empirical GMPE
584 model (Bayless and Abrahamson, 2019b) are presented for comparison purposes.

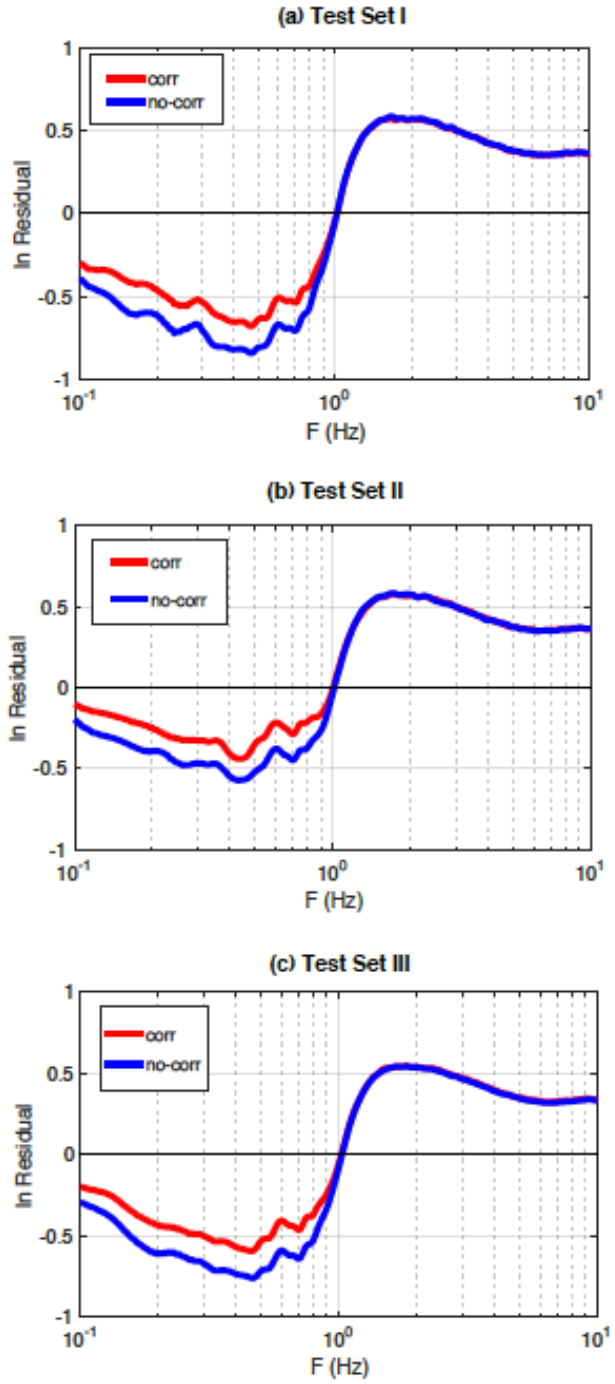

585

586 **Figure 8**. Mean residuals between the simulated EASs and those predicted by the empirical

587 GMPE (Bayless and Abrahamson, 2018b). (a) Test Set I (basic), (b) Test Set II (random

588 hypocenter), and (c) Test Set III (stress drop perturbation).

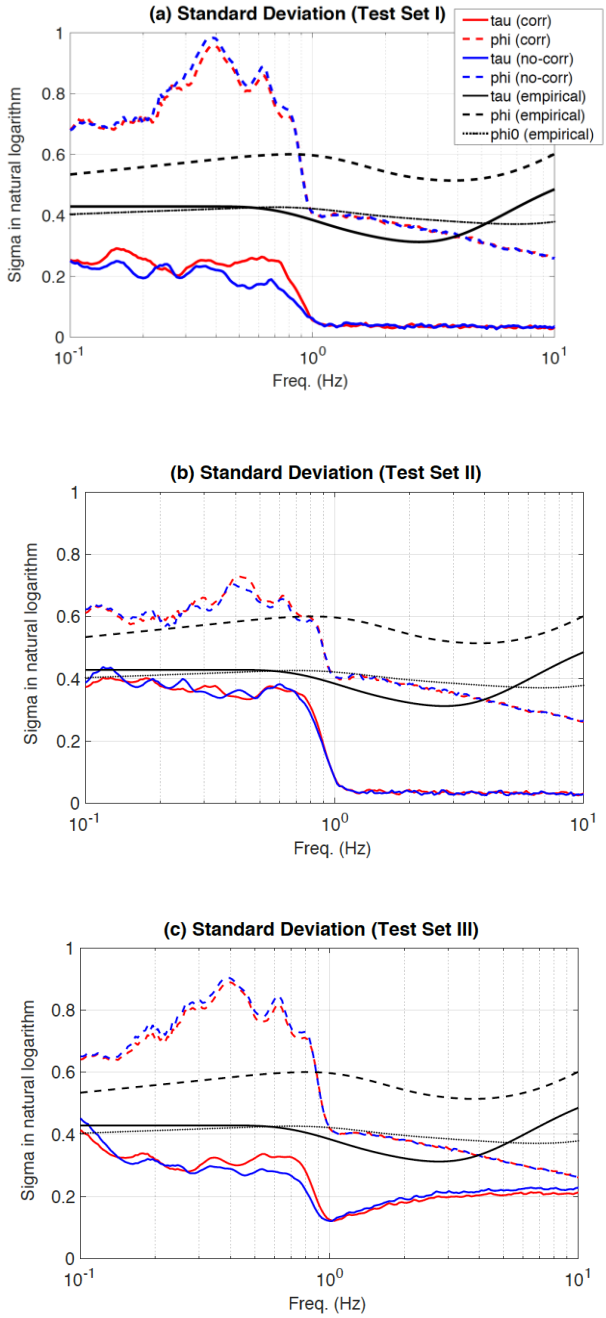

589 **Figure 9**. Standard deviations (tau: between-event, phi: within-event, and phi0: within-site) of
590 the EAS residuals in (a) Test Set I (basic), (b) Test Set II (random hypocenter), and (c) Test Set
591 III (stress drop perturbation). For the within-event standard deviation from the empirical model,
592 both the within-event (i.e., within-site and between-site terms) and only the within-site standard
593 deviations are presented for the comparison purposes.

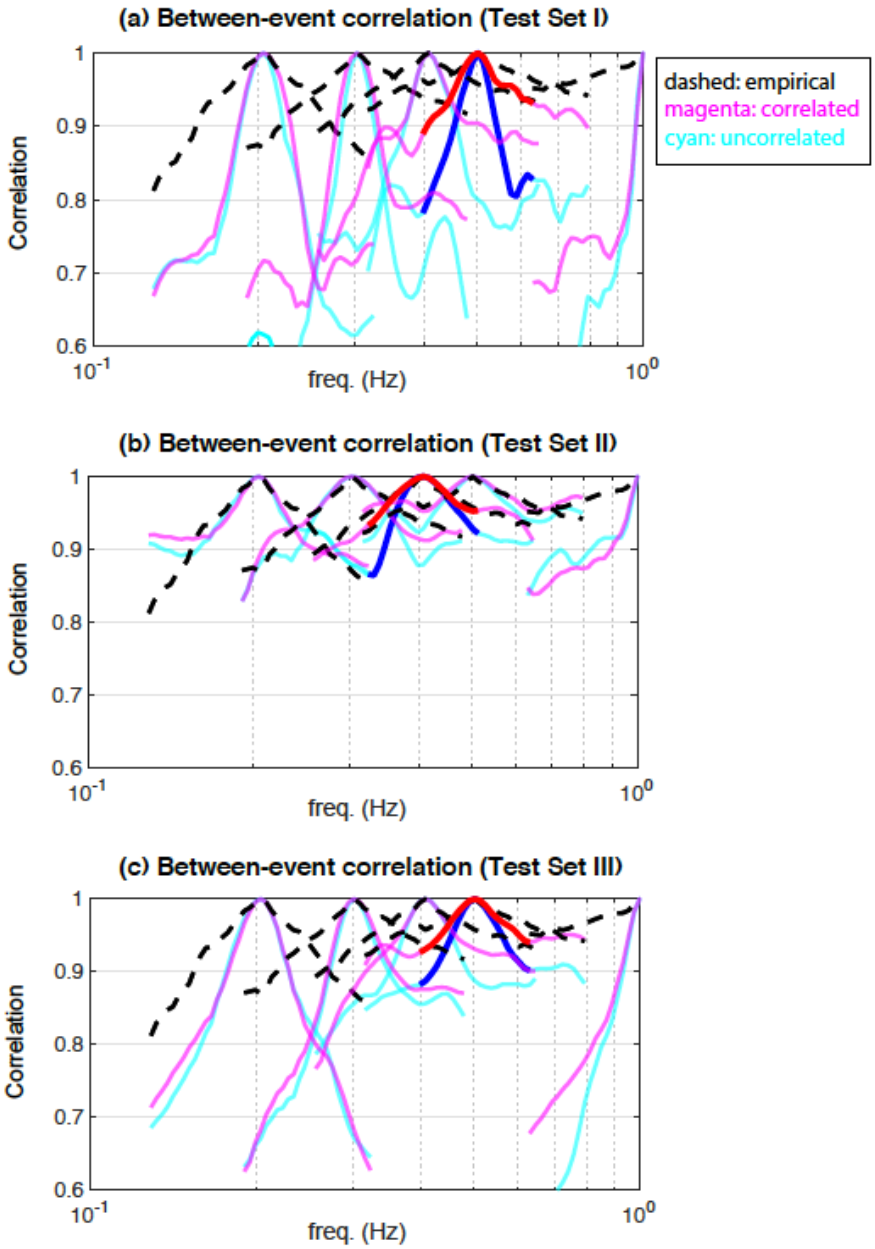

Figure 10. Inter-frequency correlations (between-event) with 5 reference frequencies (0.2, 0.3, 0.4, 0.5, and 1.0 Hz) in (a) Test Set I (basic), (b) Test Set II (random hypocenter), and (c) Test Set III (stress drop perturbation). The initial decay patterns of both correlated and uncorrelated source models from the reference frequencies, i.e., 0.5 Hz for (a) and (c), and 0.4 Hz for (b), are emphasized with red and blues lines, respectively.

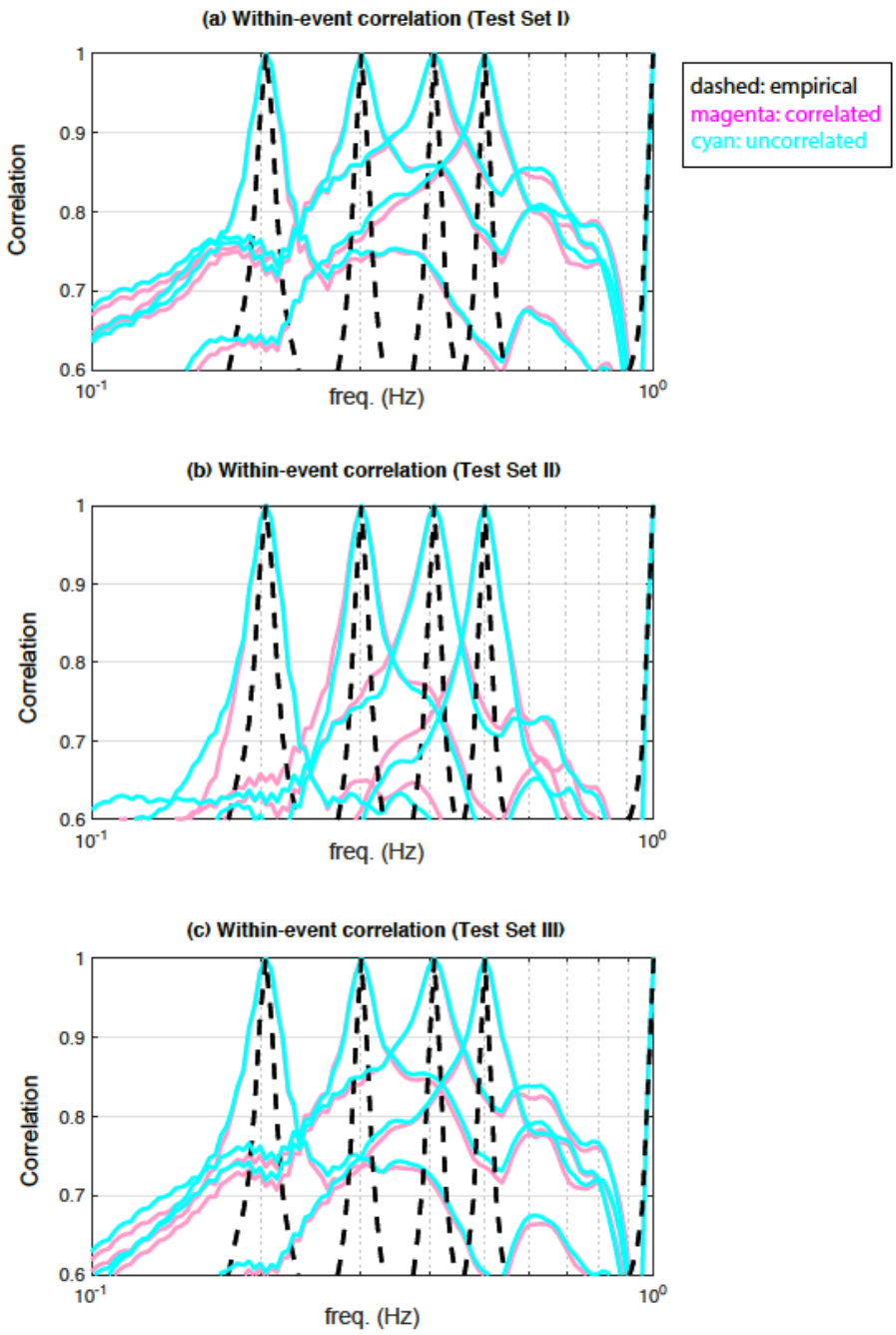

600

601 **Figure 11.** Inter-frequency correlations (within-event) with 5 reference frequencies (0.2, 0.3, 0.4,

602 0.5, and 1.0 Hz) in (a) Test Set I (basic), (b) Test Set II (random hypocenter), and (c) Test Set III

603 (stress drop perturbation).

Figure 1

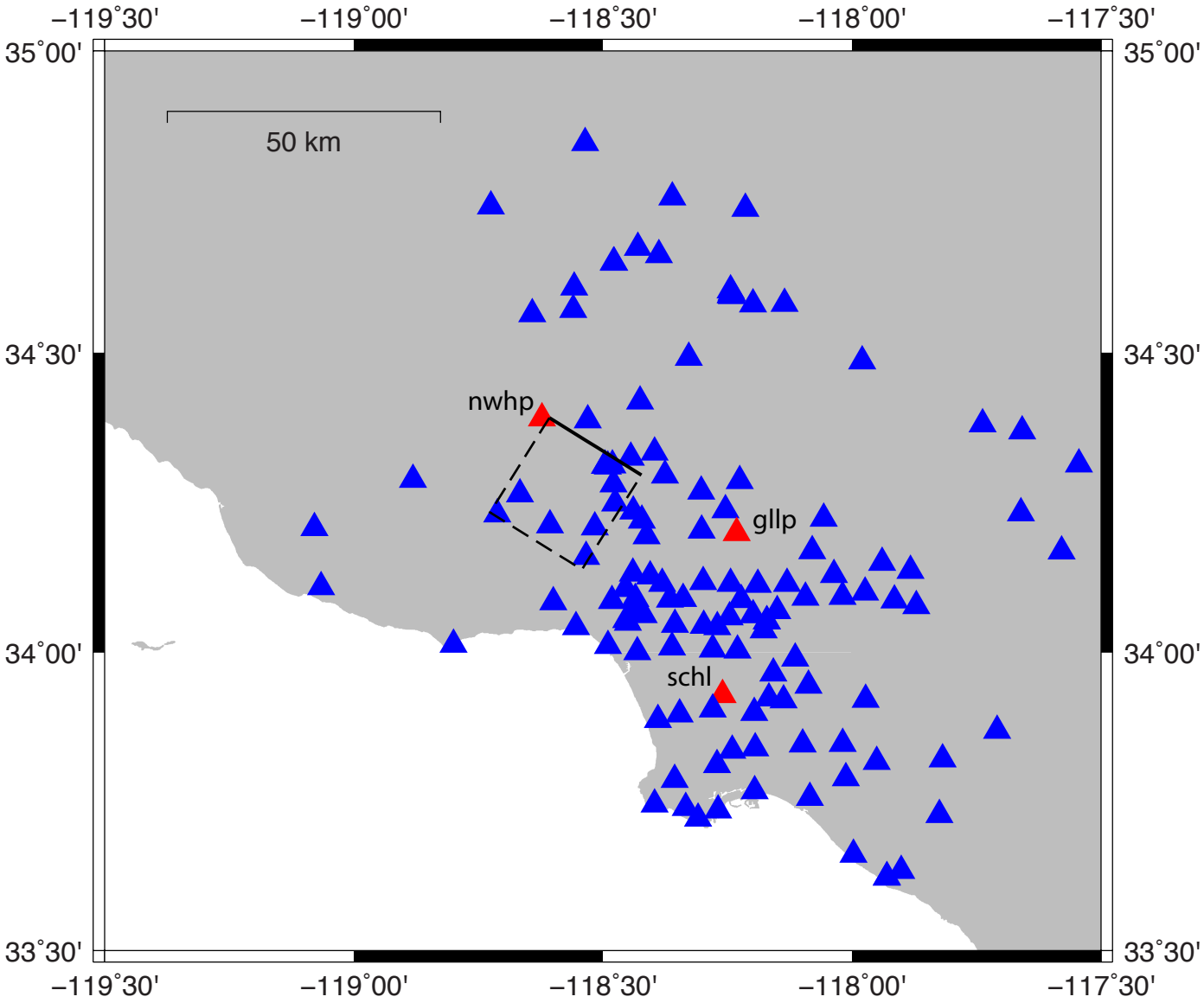
−119˚30'
−119˚00'
−118˚30'
−118˚00'
−117˚30'
35˚00'
34˚30'
34˚00'
33˚30'
50 km
nwhp
gllp
schl

Figure 2

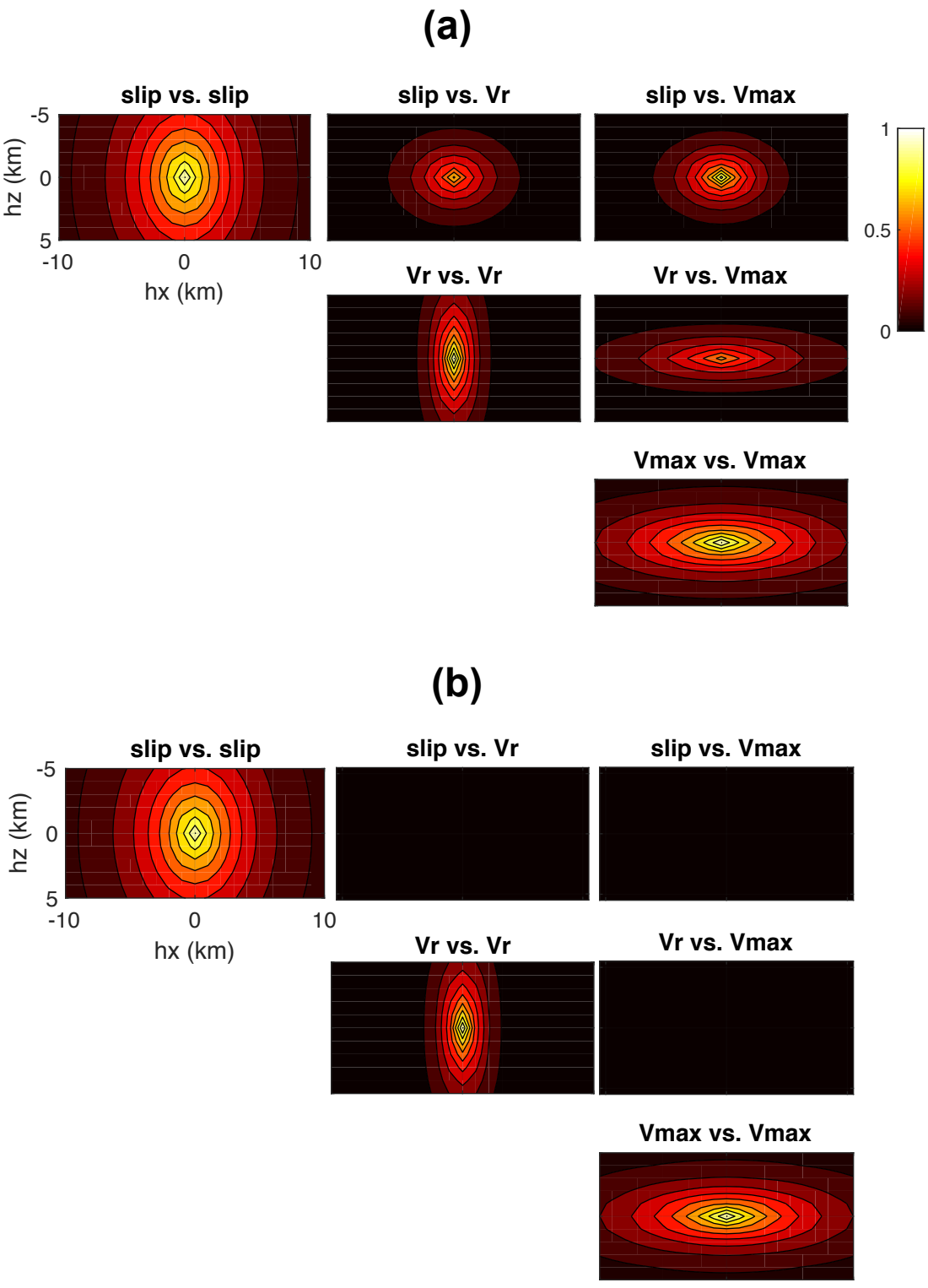
(a)
slip vs. slip
slip vs. Vr
slip vs. Vmax
Vr vs. Vr
Vr vs. Vmax
Vmax vs. Vmax
hz (km)
hx (km)
-5
0
5
-10
0
10
1
0.5
0
(b)
slip vs. slip
slip vs. Vr
slip vs. Vmax
Vr vs. Vr
Vr vs. Vmax
Vmax vs. Vmax
hz (km)
hx (km)
-5
0
5
-10
0
10

Figure 3

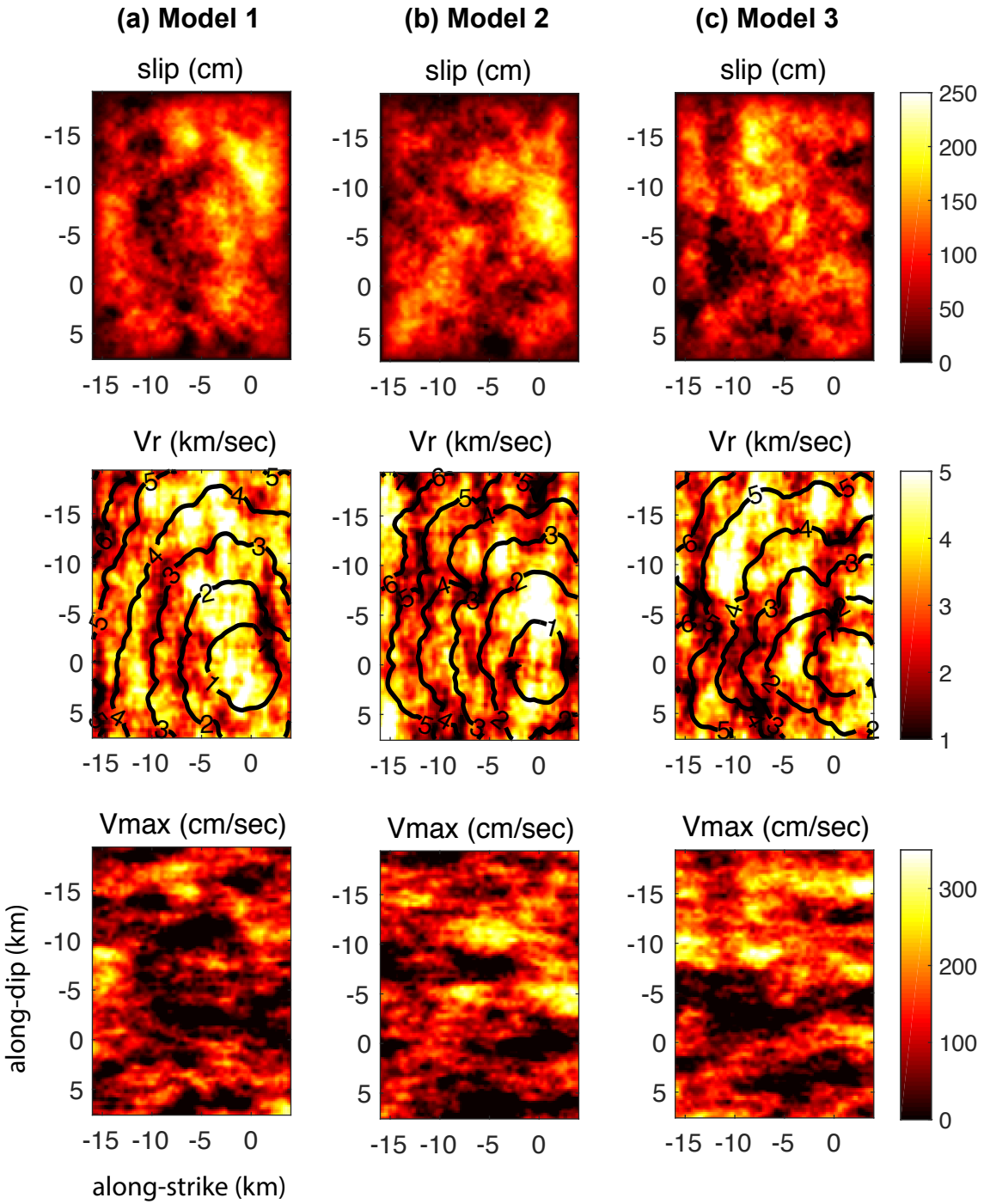
(a) Model 1
(b) Model 2
(c) Model 3
slip (cm)
Vr (km/sec)
Vmax (cm/sec)
along-dip (km)
along-strike (km)
-15
-10
-5
0
5
250
200
150
100
50
0
4
3
2
1
300

Figure 4

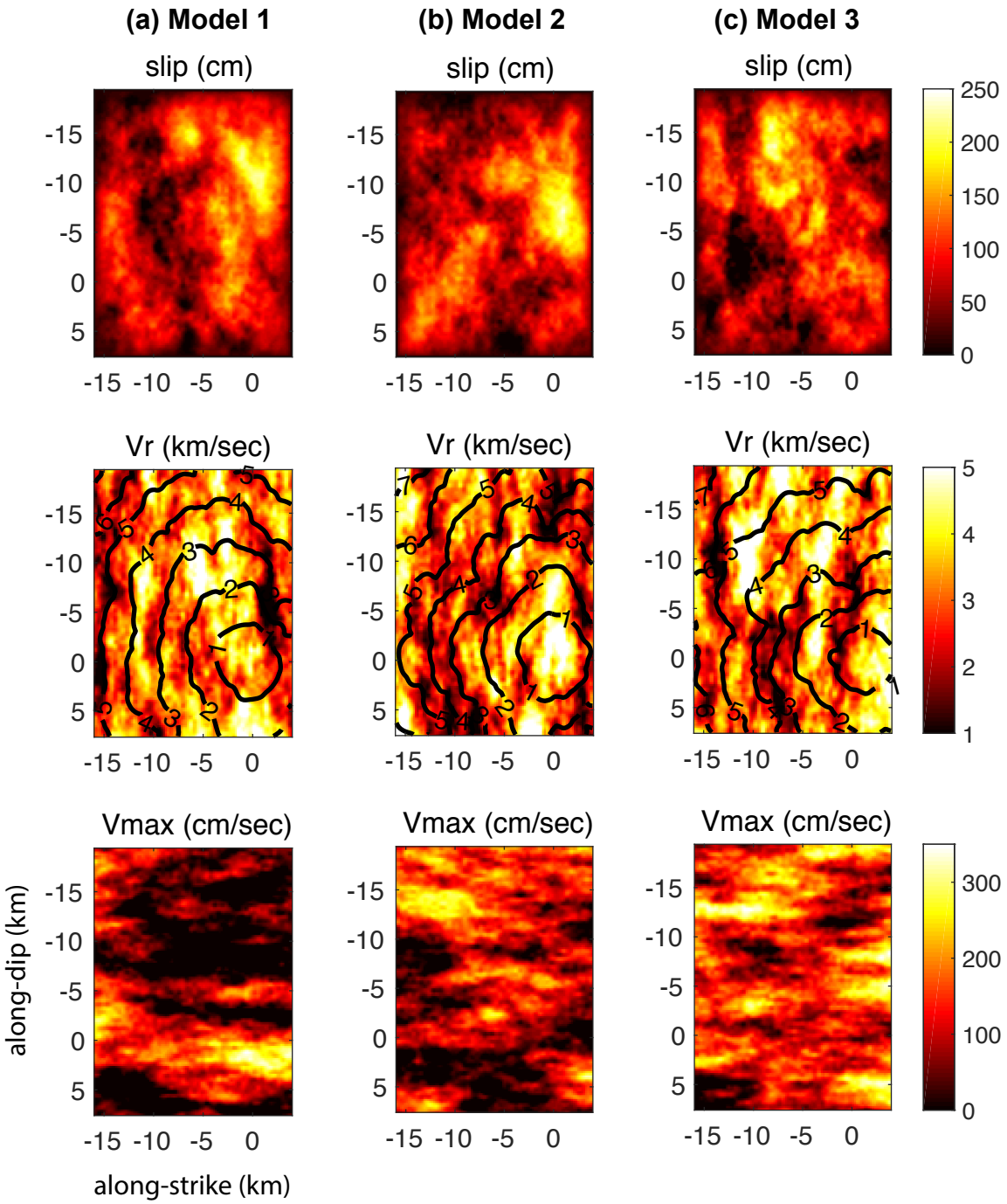
(a) Model 1
(b) Model 2
(c) Model 3
slip (cm)
Vr (km/sec)
Vmax (cm/sec)
along-dip (km)
along-strike (km)
-15
-10
-5
0
5
250
200
150
100
50
0
4
3
2
1
300

Figure 5

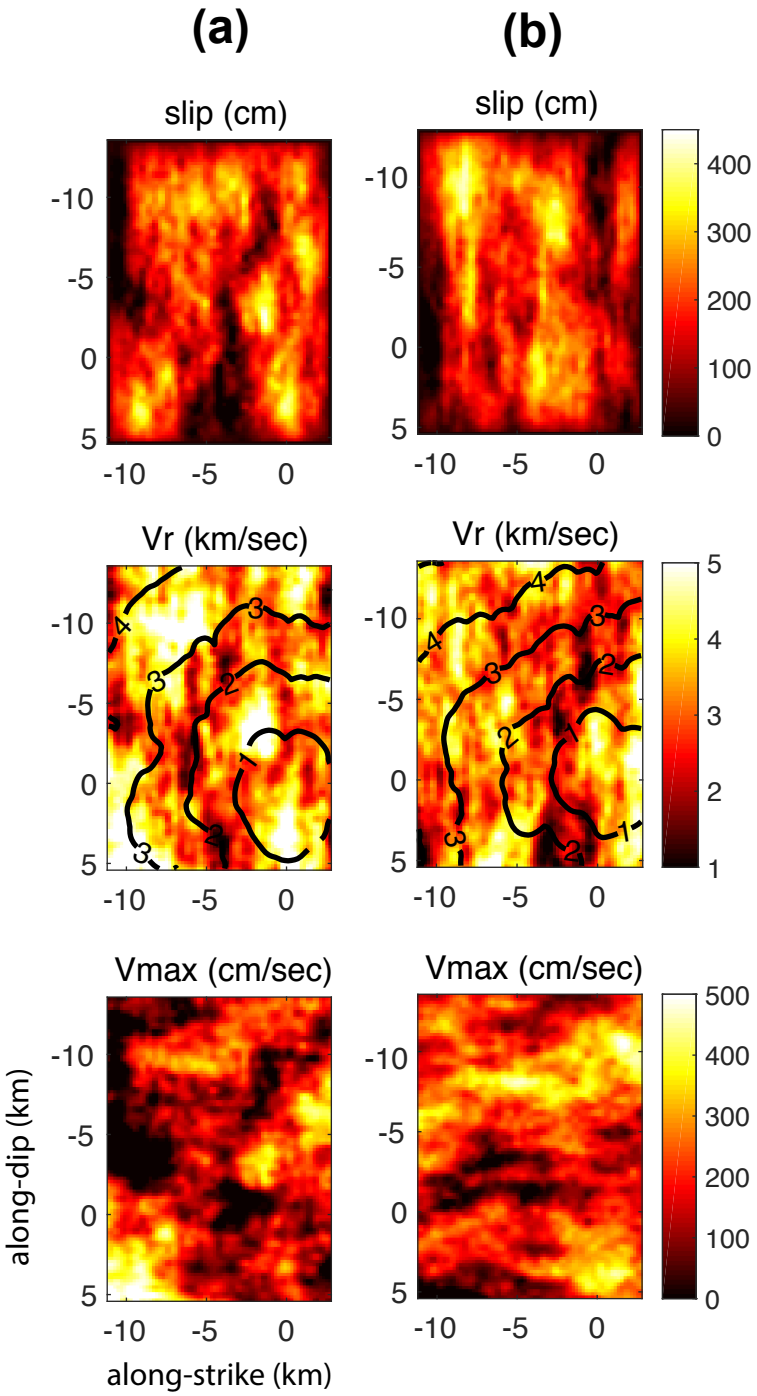
(a)
(b)
slip (cm)
slip (cm)
Vr (km/sec)
Vr (km/sec)
Vmax (cm/sec)
Vmax (cm/sec)
along-dip (km)
along-strike (km)
-10
-5
0
5
400
300
200
100
0
4
3
2
1
500

Figure 6

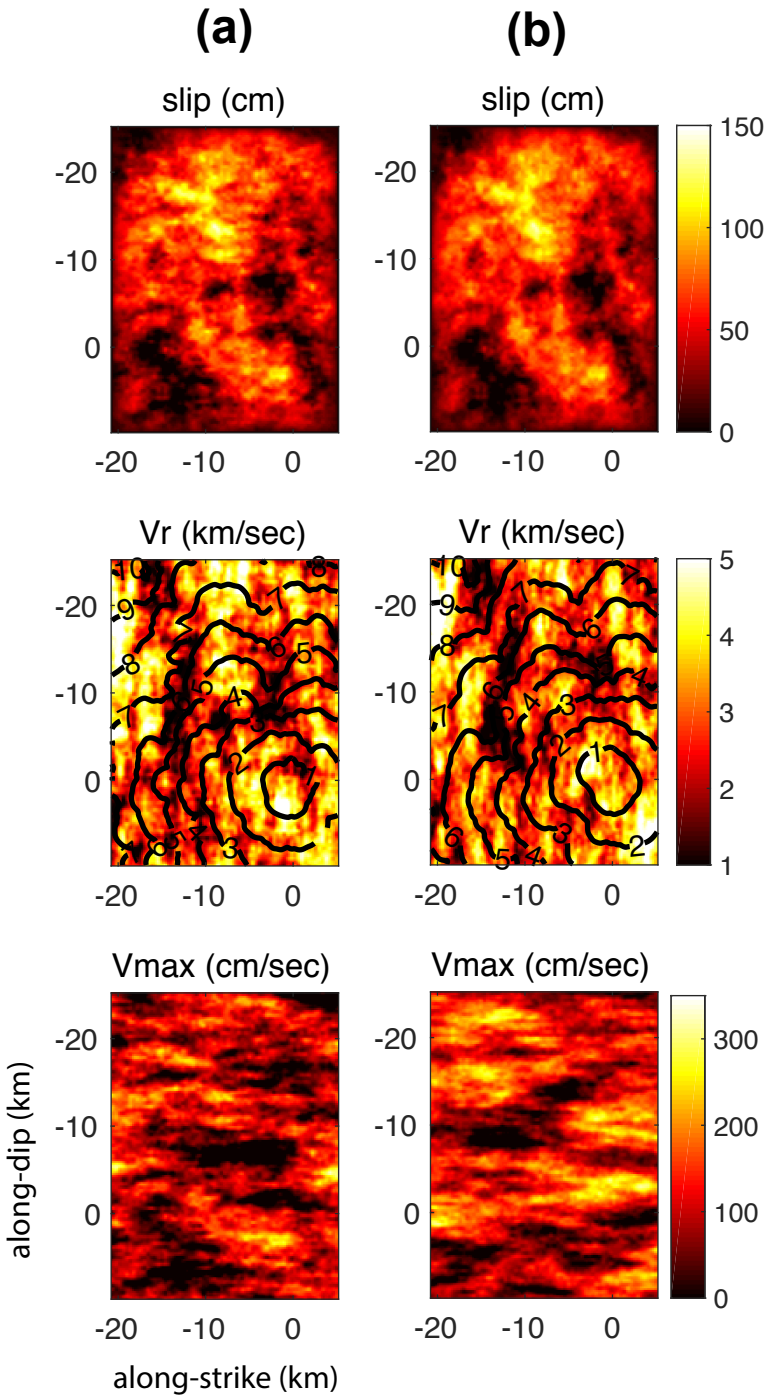
(a)
(b)
slip (cm)
slip (cm)
150
100
50
0
Vr (km/sec)
Vr (km/sec)
5
4
3
2
1
Vmax (cm/sec)
Vmax (cm/sec)
300
200
100
0
-20
-10
0
along-dip (km)
along-strike (km)

Figure 7

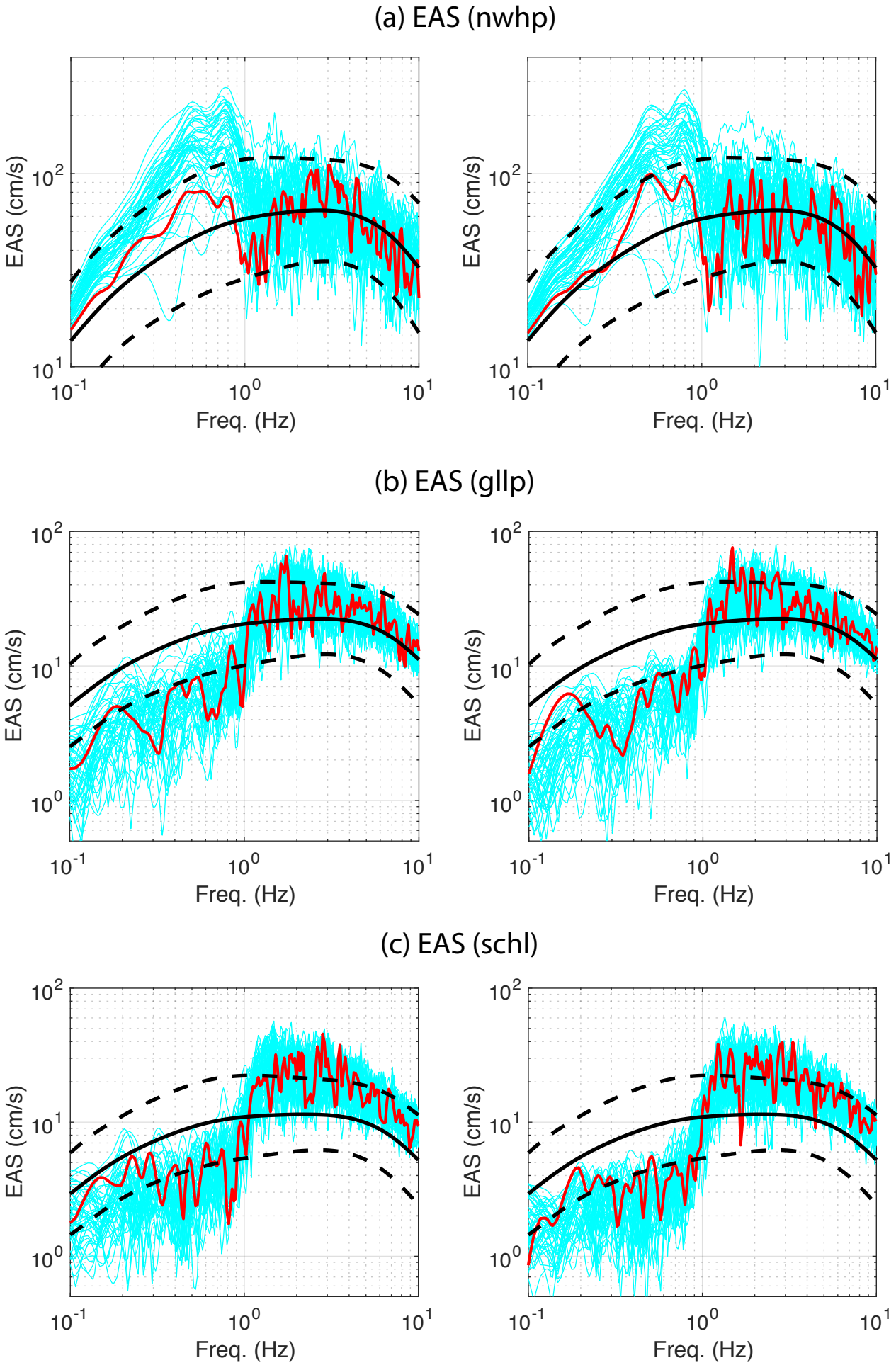

Figure 8

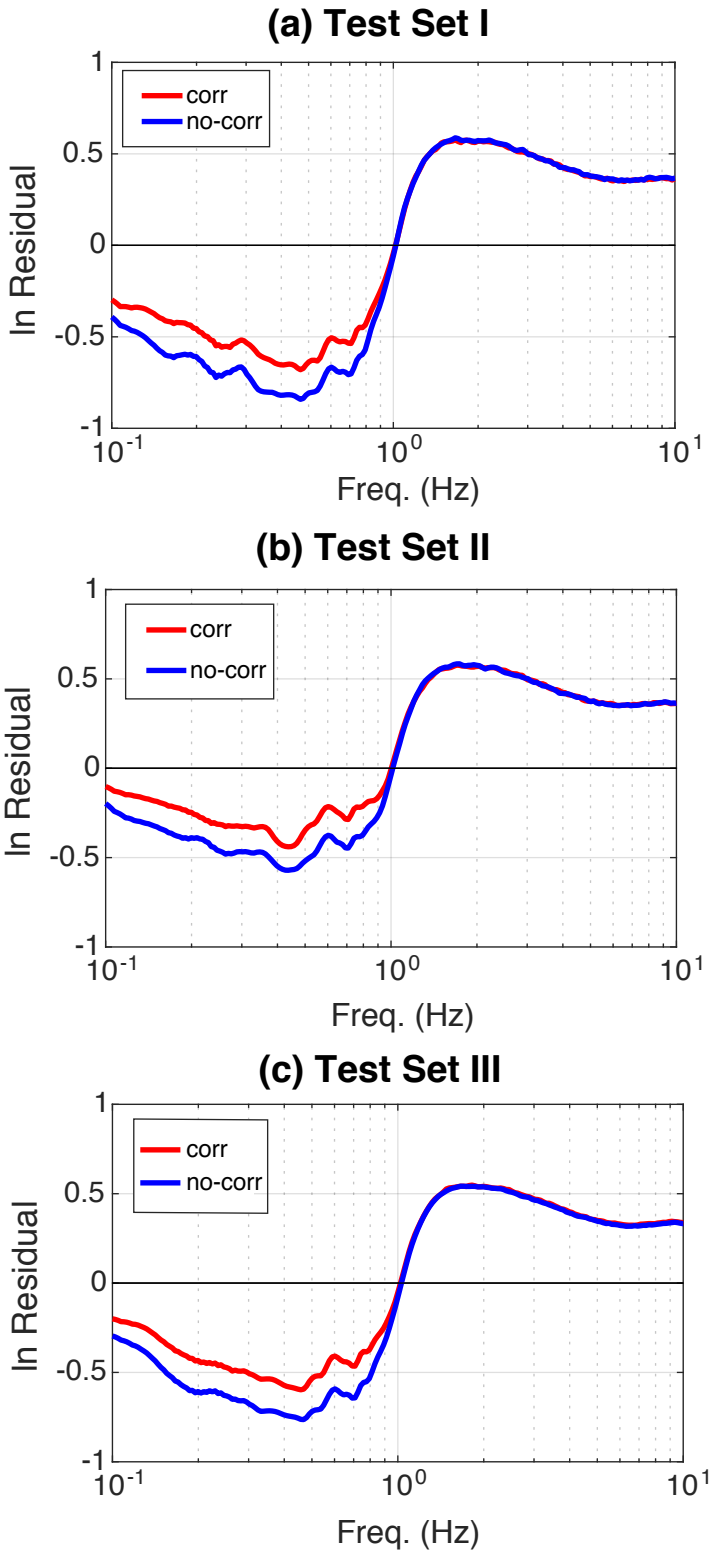
(a) Test Set I
corr
no-corr
ln Residual
Freq. (Hz)
(b) Test Set II
corr
no-corr
ln Residual
Freq. (Hz)
(c) Test Set III
corr
no-corr
ln Residual
Freq. (Hz)

Figure 9a

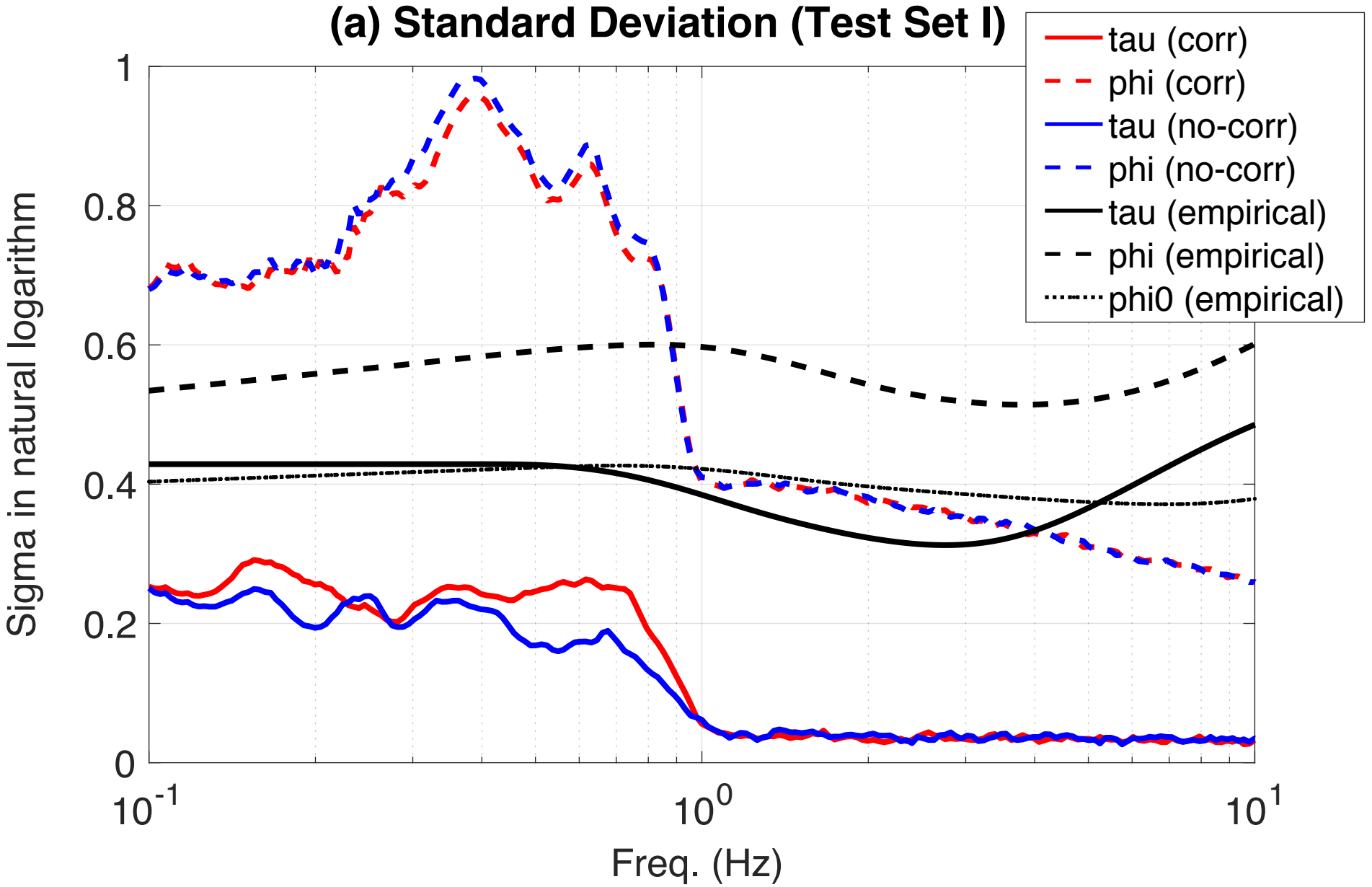
(a) Standard Deviation (Test Set I)
tau (corr)
phi (corr)
tau (no-corr)
phi (no-corr)
tau (empirical)
phi (empirical)
phi0 (empirical)
Sigma in natural logarithm
1
0.8
0.6
0.4
0.2
0
10^-1
10^0
10^1
Freq. (Hz)

Figure 9b

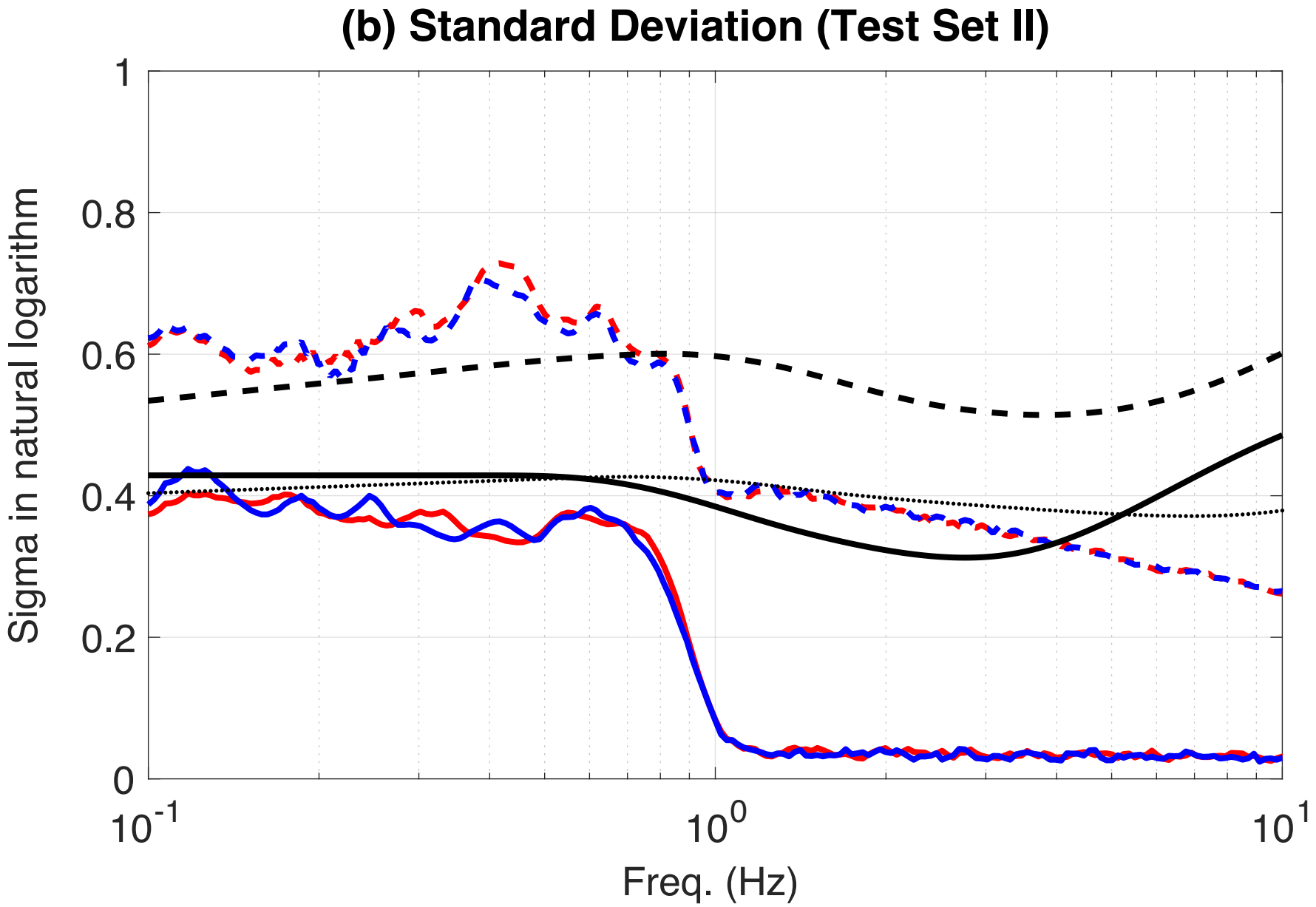
(b) Standard Deviation (Test Set II)
Sigma in natural logarithm
1
0.8
0.6
0.4
0.2
0
10^{-1}
10^{0}
10^{1}
Freq. (Hz)

Figure 9c

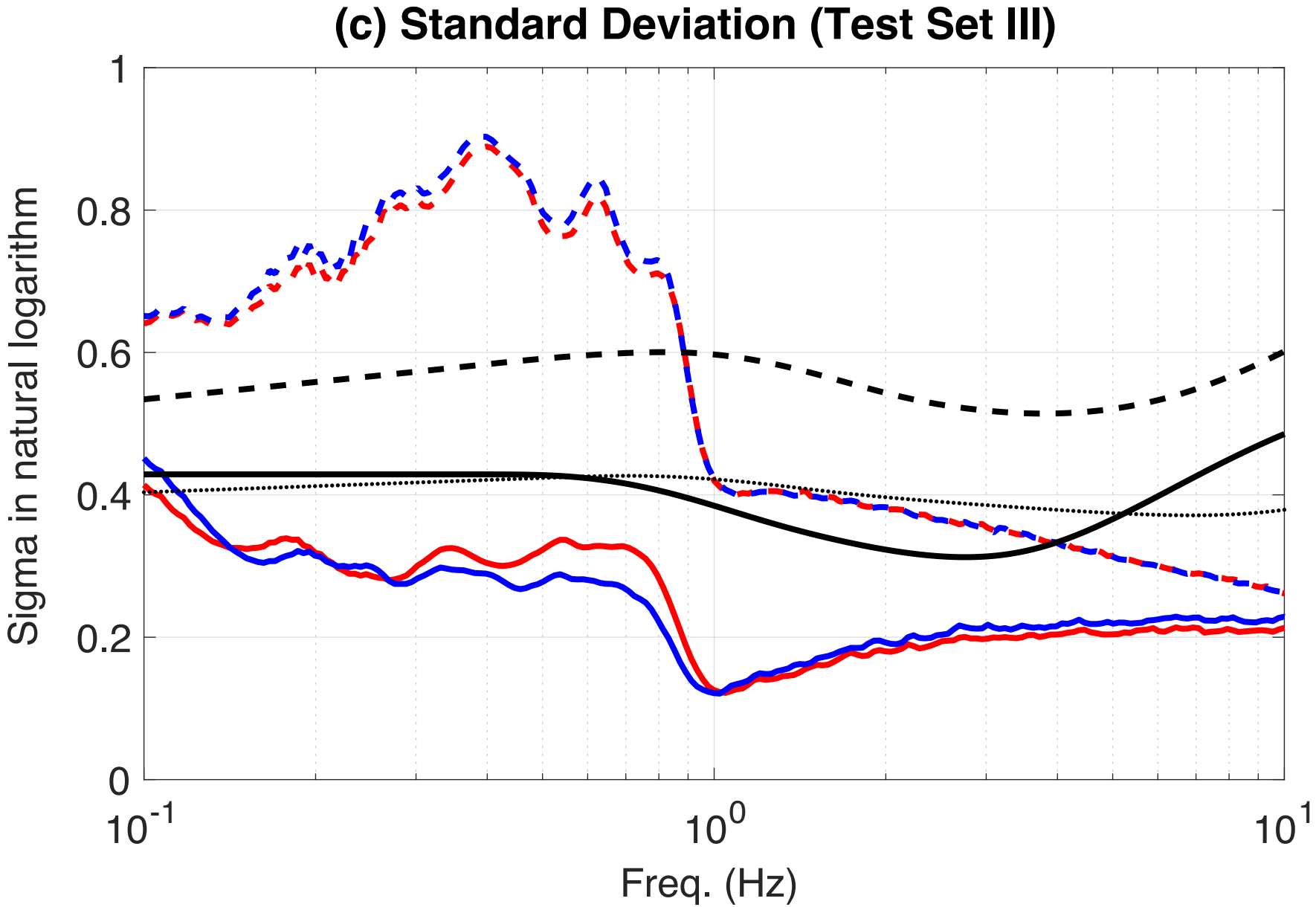
(c) Standard Deviation (Test Set III)
Sigma in natural logarithm
1
0.8
0.6
0.4
0.2
0
10^-1
10^0
10^1
Freq. (Hz)

Figure 10

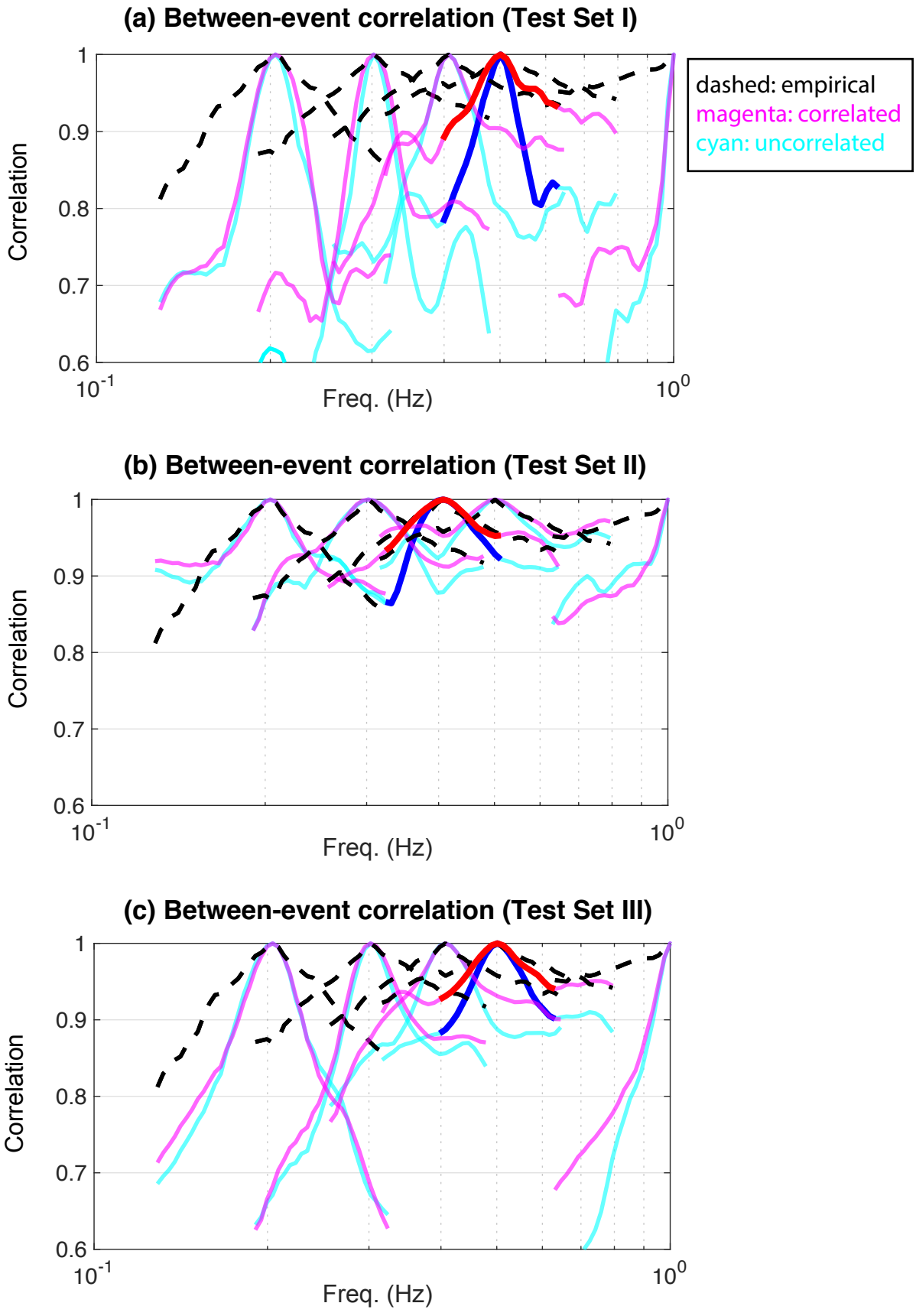
(a) Between-event correlation (Test Set I)
dashed: empirical
magenta: correlated
cyan: uncorrelated
Correlation
Freq. (Hz)
(b) Between-event correlation (Test Set II)
Correlation
Freq. (Hz)
(c) Between-event correlation (Test Set III)
Correlation
Freq. (Hz)

Figure 11

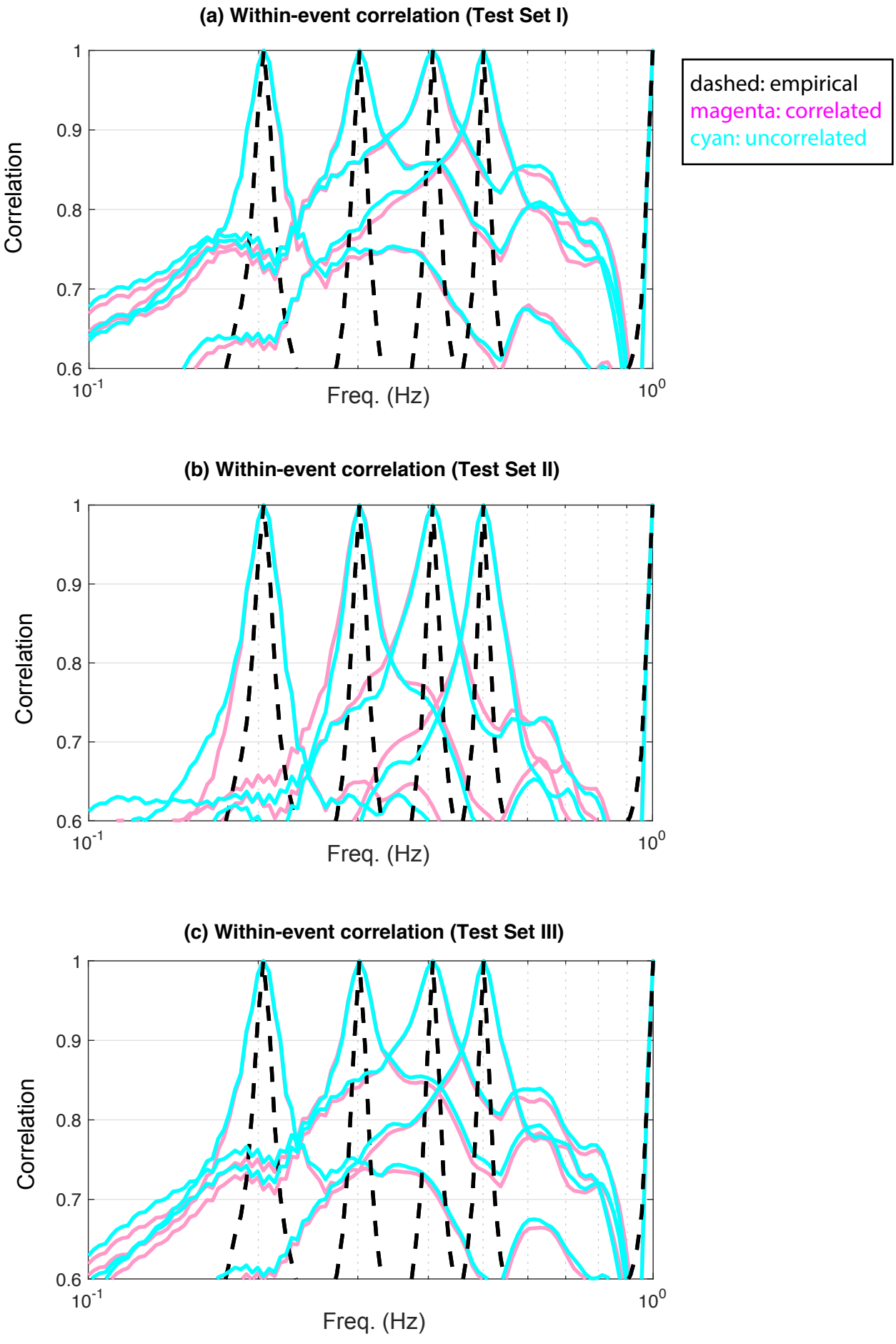
(a) Within-event correlation (Test Set I)
(b) Within-event correlation (Test Set II)
(c) Within-event correlation (Test Set III)
Correlation
Freq. (Hz)
1
0.9
0.8
0.7
0.6
10^-1
10^0
dashed: empirical
magenta: correlated
cyan: uncorrelated